

1 Seasonal and spatial pattern of dissolved organic matter

2 bio- and photodegradation in boreal humic waters

3
4 Artem V. Chupakov¹, Natalia V. Neverova¹, Anna A. Chupakova¹, Svetlana A. Zabelina¹,

5 Liudmila S. Shirokova^{1,2}, Taissia Ya. Vorobyeva¹, Oleg S. Pokrovsky^{2,3*}

6
7 ¹ Institute of Ecological Problems of the North, N. Laverov Federal Center for Integrated Arctic
8 Research, Nab Severnoi Dviny 23, Arkhangelsk 163000, Russia

9 ² Geoscience and Environment Toulouse, UMR 5563 CNRS, University of Toulouse, 14 Avenue
10 Edouard Belin, Toulouse 31400, France

11 ³ BIO-GEO-CLIM Laboratory, Tomsk State University, 35 Lenina Pr., Tomsk 634050, Russia

12
13 *corresponding author email: oleg.pokrovsky@get.omp.eu

14 Key words: bog, lake, stream, organic matter, metal, bacteria, sunlight

15
16 Synopsis:

17
18 In boreal humic waters of a forest lake and a bog, the rate of dissolved organic matter
19 photodegradation is four times higher than that of biodegradation. However, given the shallow
20 (0.5 m) light-penetrating layer, the biodegradation provides the largest contribution to CO₂
21 emission from water surfaces. A few trace metals were partially removed (1-10 %) during photo-
22 and biodegradation, via precipitation of Fe(III) hydroxides after destabilization of organo-ferric
23 colloids and organic complexes

24
25 Submitted to *Biogeosciences*, after 2nd revision August 2024

33 **Abstract**

34 Studying competitive effects of microbial and light-induced degradation of dissolved organic
35 matter (DOM) and trace metals is crucially important for understanding the factors controlling
36 aquatic carbon (C), micronutrients and toxicants transformation in boreal waters. Here we
37 characterized the degree of DOM and related major and trace element transformation under biotic
38 activity and sunlight using conventional incubations of humic surface waters from the European
39 subarctic: an ombrotrophic peatbog continuum (subsurface water – peatland pool – stream) and
40 a stratified forest lake across seasons. Along the bog water continuum, biodegradation rate was
41 the highest in subsurface waters collected via piezometer and the lowest in the acidic peatland
42 pool. Photodegradation was similar for piezometrically collected subsurface waters and the
43 stream, but was not detectable in the peatland pool. The waters of forest lake exhibited a strong
44 seasonal effect of biodegradation, which was the highest in October and the lowest in June.
45 Overall, the biodegradation was capable of removing between 1 and 7 % of initial DOC, being
46 the highest in the forest lake in October and in peatland pool in summer. The photolysis was
47 capable of degrading a much higher proportion of the initial DOC (10-25 %), especially in the
48 forest lake during June and the bog stream during July. Only a few trace metals (TM) were sizably
49 affected by both photo- and biodegradation of DOM (Fe, Al, Ti, Nb and light REE), whereas V,
50 Mn, Co, Cu and Ba were affected solely by biodegradation. A likely mechanism of metal removal
51 was their coprecipitation with coagulating Fe(III) hydroxides. Compared to typical CO₂
52 emissions from inland waters of the region, biodegradation of DOM can provide the totality of
53 C-CO₂ evasion from lake water surfaces whereas bio- and photodegradation are not sufficient to
54 explain the observed fluxes in bog water continuum. Overall, these results demonstrated strong
55 spatial and seasonal variability in bio- and photodegradation of DOM and organic TM
56 complexes, and call for the need of a systematic assessment of both processes across seasons
57 with high spatial resolution.

58 **1. Introduction**

59 Organic Carbon (OC) processing via metabolic biological (heterotrophic bacteria uptake
60 and respiration) and inorganic physico-chemical (photolysis) pathways is considered to be one
61 of the major source of CO₂ supersaturation in surface waters and related C emissions (Lapierre
62 et al., 2013; Tranvik et al., 2009), although the relative role of dissolved vs particulate organic
63 carbon (DOC and POC, respectively) remains poorly quantified (e.g. Attermeyer et al., 2018;
64 Lau et al., 2021; Shirokova et al., 2021; Keskitalo et al., 2022; Raudina et al., 2022). Given
65 sizable CO₂ emissions in boreal and subarctic waters (Karlsson et al., 2021), together with high
66 concentrations of DOC (Cole et al., 2007; Vonk et al., 2015), and fast ongoing and predicted
67 environmental changes in high latitude aquatic and terrestrial ecosystems (Wauthy et al., 2018;
68 Chaudhary et al., 2020; Harris et al., 2022), the surface waters of subarctic regions are at the
69 forefront of studies on the biogeochemical cycle of C. Although emissions from these waters are
70 significantly lower than those in the 10 °S – 10 °N equatorial belt (e.g., Borges et al., 2015), the
71 magnitude of possible changes in C flux from northern waters to the atmosphere remains much
72 less known. Further, there are still important geographical biases linked to insufficient knowledge
73 of rates and mechanisms of DOC transformation in certain regions. An example is wetland-
74 dominated northern aquatic settings, where high concentrations of soil organic C surrounding the
75 bogs provide high concentrations of DOC but also some related trace metals, whose
76 concentration and migration can be strongly controlled by processes of dissolved organic matter
77 (DOM) transformation.

78 Thorough laboratory and field work on DOM bio- and photolability conducted over the
79 past decades have demonstrated both phenomena are important, and, depending on
80 environmental setting (nutrient regime, photic layer depth, nature of DOM, etc.), one or another
81 may dominate overall DOM removal in surface waters (Vachon et al., 2016, 2017; Vähätalo and
82 Wetzel, 2008; Obernosterer and Benner, 2004). In addition to DOM, trace elements (limiting

83 micronutrients, toxicants and geochemical tracers) present in the form of organic and organo-
84 mineral (Fe, Al) colloids and organic matter complexes may be subjected to strong transformations
85 during microbiological and photolytic degradations of DOM. This in turn may impact the
86 bioavailability, toxicity and export fluxes of trace metals in from terrestrial to aquatic continental
87 and finally coastal environments.

88 Recently, specific attention was devoted to the aquatic systems of permafrost peatlands
89 given their high vulnerability to climate warming and huge potential for release of soil organic
90 C to surface waters (Vonk et al., 2015; Shirokova et al., 2019; Payandi-Rolland et al., 2020;
91 Prijac et al., 2022; Rosset et al., 2022; Taillardet et al., 2022). These studies provided a range of
92 DOM susceptibility to biotic degradation. Thus, between 10 and 40 % of the DOC in lakes, rivers
93 and soil waters of the boreal zone may be available for bacterial uptake over a time frame of
94 several weeks (Berggren et al., 2010; Roehm et al., 2009). This range is consistent with 14-16%
95 of biodegradable DOC (BDOC) assessed globally (Begum et al. 2022). The necessity for further
96 studies was also indicated, most notably with regard to *i*) seasonal aspects, given that the
97 overwhelming majority of available studies were performed during Arctic summer (see
98 discussions in Vonk et al., 2015; Laurion et al., 2021), and *ii*) increased spatial resolution, given
99 that sizable variations of BDOC can be observed within quite short distances of a hydrological
100 continuum (Payandi-Rolland et al., 2020; Raudina et al., 2022). Another poorly studied aspect is
101 DOM photo- and biolability across the depth of the water column, especially in seasonally
102 stratified lakes which are subject to spring and autumn overturn.

103 Based on a compilation of available studies on BDOC and their own research, Vonk et
104 al. (2015) argued there is a negligible amount of biodegradable DOC in aquatic systems without
105 permafrost. This is, however, contradictory to available assessments on biodegradation of aquatic
106 DOM as major driver of CO₂ emission in general (Amaral et al., 2021; Liu and Wang, 2022) and
107 in boreal waters in particular (Ask et al., 2012; Lapierre et al., 2013). Furthermore, among all

108 Arctic rivers, the highest annual (20%) and winter (ca. 45%) biodegradable DOC (BDOC) was
109 reported for the Ob River, which drains through peatlands with minimal permafrost influence
110 (Wickland et al., 2012). These non-exhaustive examples illustrate certain inconsistency in
111 current estimations of DOC biodegradability in surface organic-rich waters of high latitudes,
112 which precludes quantitative modeling of future C fluxes between land, water and atmosphere in
113 these environmentally important regions. Towards addressing these inconsistencies, in this study,
114 we chose a typical hydrological continuum in a boreal ombrotrophic bog in a glacial lake-ridge
115 complex that includes subsurface water, a small peatland pool in the central part of the bog and
116 an outlet stream. Further, we selected a well-studied deep stratified humic lake in the same region
117 (Lake Temnoe; Chupakov et al., 2017) where we sampled surface and deep horizons for the
118 incubation experiments. The chosen waters represent subarctic non-permafrost regions that
119 exhibit sizable organic C pool in their soils and high concentrations of DOC in their surface
120 waters. In contrast to previous studies of permafrost peatlands (Shirokova et al., 2019; Laurion
121 et al., 2021; Payandi-Rolland et al., 2020; Mazoyer et al., 2022) where the main source of DOM
122 is peat or ground vegetation like mosses and lichens, in this highly productive southern taiga
123 region, DOC may be more vulnerable to microbial activity due to the presence of forest leachates
124 (i.e., Don and Kalbitz, 2005; Kalbitz et al., 2003; Kawahigashi et al., 2004; Kiikkilä et al., 2013)
125 and much higher bioproductivity for both the terrestrial and aquatic parts of the lake-river
126 ecosystems. A broad importance of DOM bio- and photodegradation dynamics is that these
127 processes can contribute to CO₂ emissions from water surfaces thereby directly controlling the
128 C cycling between the land and the atmosphere.

129 The first working hypothesis behind our study design is that the DOC-rich subsurface
130 water and deep horizons of the humic lake are mostly sensitive to sunlight impact (Stubbins et
131 al., 2010), and that maximal impact of photodegradation is expected during allochthonous
132 aromatic DOM input (high surface inflow to lakes and bogs in June and October). In contrast,

133 maximal biodegradation of DOM is expected during periods of possible phytoplankton bloom in
134 August, when autochthonous organic material is generated in the water column. An important
135 novelty of the present study is addressing trace metal (TM) partitioning during bio- and
136 photodegradation. The link between DOM and TE is straightforward: in humic waters of
137 peatlands, most TE (except probably some alkalis and oxyanions) are strongly (> 80%)
138 associated to DOM in the form of organic and organo-mineral (Fe, Al) colloids (Pokrovsky et
139 al., 2005, 2012, 2016). As a result, any DOM transformation processes may directly control the
140 pattern of TE. From the other hand, some TE may be photosensitive (Mn, Fe), toxic (Al, Cu, As,
141 Cd, Pb), or limiting micronutrients (Zn, Co, Ni, Mo) for the bacteria. Our second working
142 hypothesis here is that removal of DOM via photo- or bio-degradation will change the
143 partitioning of trace elements which are either *i*) strongly bound to DOM, such as divalent
144 transition metals, or *ii*) incorporated into organo-mineral (Fe, Al) colloids, such as trivalent and
145 tetravalent hydrolyses. The TE of 1st group might either remain in solution (during
146 photodegradation), hence not modifying their total dissolved concentration, or being taken up by
147 growing bacteria during bio-degradation of TE-bound organic matter (Shirokova et al., 2017a,
148 c). The elements of the second group are capable of co-precipitating with Fe and Al hydroxides
149 hence being scavenged from the aqueous solution.(e.g., Kopacek et al., 2005, 2006). To test
150 these hypotheses, we examined DOM and related trace metals bio- and photodegradability
151 aiming to assess 1) spatial variations along a hydrological continuum of non-permafrost peatland
152 and different horizons of a neighboring deep stratified lake located in the forest, and 2) temporal
153 variability during 3 main hydrological seasons (high flow in June, baseflow in August and
154 autumn rain season in October) in the forest lake. Achieving these objectives should allow
155 quantifying the relative share of bio- and photodegradation on overall DOC and TM removal
156 from surface waters via biotic and physico-chemical mechanisms. The third aim of this study

157 was to relate the measured rates of DOM photo and biodegradation to CO₂ emissions observed
158 in the studied water bodies.

159

160 **2. Materials and Methods**

161 *2.1. Natural settings of subarctic bog and stratified lake*

162 The study site is in the NE part of the European boreal zone (Arkhangelsk region), **Fig.**

163 **1.** The mean annual air temperature is 0 °C and average annual precipitation is 700 ± 50 mm.

164 The pristine ombrotrophic Ilaskoe Bog is located 30 km SE of Arkhangelsk, and is a typical

165 lake-ridge complex formed from the last glaciation approximately 10,000 years ago. Its total

166 surface area is 89 km², with an average peat thickness of 3 m. The hydrological continuum of the

167 Ilaskoe Bog includes subsurface water collected via piezometer (2-2.5 m depth), a small lake

168 (Severnoe) and a stream outlet (**Fig. 1**). Lake Severnoe, located in the central part of the bog, is

169 a typical peatland pool with an average depth of 1.5 m and a surface area of 0.013 km². The

170 Chernyi Stream is an outlet for the eastern part of the bog. The stream is 0.7-2.0 m wide, 10 km

171 long and it flows in a forested (taiga) zone in the shade of tree canopy. The waters of the Ilaskoe

172 Bog are acidic (pH ranges from 3.9-4.0 in piezometer and peatland pool to 5.7 in stream Chernyi),

173 organic-rich (DOC is equal to 88, 13 and 38 mg L⁻¹ in the piezometer, lake and stream,

174 accordingly) and low mineralized (Electrical Conductivity is 17-46 μS cm⁻¹), as listed in **Table**

175 **1.**

176 Lake Temnoe is located in a pristine forest 100 km NNE of the town of Arkhangelsk, an

177 area that does not receive any direct anthropogenic impact (**Fig. 1**). The watershed area is 3.08

178 km² and the lake surface area is 0.091 km², with a maximum depth of 37 m and a Secchi disk

179 depth of 3.5±0.5 m. The water residence time in the lake is 394 days. Bogs constitute 31% of

180 lake's watershed area, which is represented by carbonate-free loamy moraine atop the peat,

181 podzol and gley soils. The lake water is slightly acidic (pH = 5.1 to 6.0), humic (DOC = 13-20

182 mg L⁻¹) and dominated by allochthonous DOM with a low concentration of total dissolved ions
183 (Electrical Conductivity of 20 µS cm⁻¹). Similar to other deep boreal and subarctic lakes, the lake
184 exhibits 2 main periods of pronounced stratification (November to April and June to September)
185 and two periods of lake overturn (October and May). Maximal winter stratification occurs in
186 March; the highest water temperature typically occurs in July (see Chupakov et al., 2017 for
187 details).

188 The surface waters were collected from the shore (peatland pool and stream) or a PVC
189 boat (Lake Temnoe). Surface (30-50 cm depth) waters were sampled in the Ilasskoe bog and 3
190 water horizons (0.5, 5 and 10 m) were sampled in the Temnoe Lake using a pre-cleaned
191 polycarbonate horizontal water sampler (Aquatic Research Co, ID, USA). The water samples
192 were placed into 2-L Milli-Q pre-cleaned PVC jars and kept refrigerated (4 °C) until arrival at
193 the laboratory within 2-3 hours of collection.

194

195 *2.2. Experiments*

196 2.2.1. Biodegradation

197 For DOM biodegradation assessments we followed the recommended protocol and used
198 the appropriate type of labware for assessing biodegradable DOC of Arctic waters without
199 external nutrient addition (Vonk et al., 2015; Payandi-Rolland et al., 2020) and applied a slight
200 modification from Shirokova et al. (2019) to assess maximal possible biodegradation. Initial
201 water samples brought to the laboratory within 2-3 hours after sampling were filtered through 3
202 µm sterilized Nylon Sartorius membranes (47 mm diameter); these were used because
203 ‘conventional’ 0.8-1.2 µm (GF/F) filtration membranes might remove too many microbial cells
204 (Dean et al., 2018).

205 Duplicate 30 mL aliquots of 3 µm-filtered water were placed into pre-combusted (4.5
206 hours at 450°C) dark borosilicate 40 mL glass bottles wrapped in Al foil to prevent any

207 photolysis, without nutrient amendment and incubated at $22\pm 1^\circ\text{C}$ in the dark. The bottles were
208 closed with loosened sterilized PVC caps to allow air exchange. The bottles were shaken
209 manually once a day avoiding the liquid touching the cap. The entire reactor was used for
210 sampling after 0, 2, 5, 8, 12, and 21 days of exposure. Sampled solutions were filtered through
211 sterile, MilliQ-cleaned Sartorius $0.22\ \mu\text{m}$ filters. The DOC blanks for these filters did not exceed
212 1% of DOC concentrations in experimental samples. Sterilized control reactors were filled with
213 natural water that was filtered through a $0.22\ \mu\text{m}$ sterile filter and incubated together with
214 experimental reactors following the approach of Köhler et al (2002).

215 All handling and sampling of bottles was performed in the laminar hood box in a sterilized
216 workspace. Filtered samples were acidified with $30\ \mu\text{L}$ of concentrated (8.1 M) double distilled
217 HCl, tightly capped and stored in the refrigerator before DOC analyses. The non-acidified portion
218 of filtrate was used for pH, Specific Conductivity, DIC and $\text{UV}_{254\ \text{nm}}$ and optical spectra
219 measurement. Control runs were $0.22\ \mu\text{m}$ sterile-filtered water which was incubated in parallel
220 with experiments and re-filtered through $0.22\ \mu\text{m}$ filters the day of sampling. To ensure
221 minimized release from sterilized Nylon membrane, we ran blank (Milli-Q) filtrations through
222 both GF/F and $0.22\ \mu\text{m}$ Nylon filters; in both cases the DOC blank was below 0.1-0.2 mg/L
223 which is less than 1% of DOC concentration in our samples. The glass bottles were incubated in
224 duplicates at $22\pm 1^\circ\text{C}$ and agitated manually at least once a day over the 16 days of exposure.

225

226 2.2.2. Photodegradation

227 For photodegradation incubations, water samples were collected in Al-foil covered pre-
228 cleaned polypropylene jars and sterile filtered ($0.22\ \mu\text{m}$ Nalgene Rapid-Flow Sterile Systems)
229 within 2 hours of sampling and refrigerated. The filtrates were transferred under laminar hood
230 box into sterilized, acid-washed quartz tubes (150 mL volume, 20% air headspace) with silicate
231 stoppers and placed at $3 \pm 2\ \text{cm}$ depth into an outdoor pool which was filled by river water having

232 the light transparency similar to that of the Illasskoe and Temnoe lakes. The outdoor pools were
233 placed in an unshaded area with a latitude similar to the sampling sites (< 30 km from Illasskoe
234 Bog and Temnoe Lake). Slight wind movement and regular manual shaking allowed for
235 sufficient mixing of reactor interiors during exposure. All photodegradation experiments were
236 run in duplicates. The water temperature (EBRO EBI 20) and light intensity (Luxmeter Testo
237 545) were continuously recorded every 3 hours.

238 For DOM photodegradation experiments, we followed conventional methods requiring
239 exposure of 0.2 μm -sterile filtered samples in quartz reactors in the outdoor pool (Vähätalo et
240 al., 2003; Chupakova et al., 2018; Gareis and Lesack, 2018), solar simulator (Lou and Xie, 2006;
241 Amado et al., 2014) or directly in the lake water (Laurion and Mladenov, 2013; Groeneveld et
242 al., 2016). Note that the 0.22 μm sterile filtration is the only way of conducting photodegradation
243 experiments, given that autoclave sterilization of DOM-rich natural waters would coagulate
244 humic material and thereby would not be suitable (Andersson et al., 2018). Filtration through a
245 smaller pore size, however, would decrease the concentration of DOC and trace metals (i.e., Ilina
246 et al., 2014; Vasyukova et al., 2010). We have chosen a 16 day exposure time for logistical
247 constraints, which is still consistent with biodegradation experiments described above and with
248 the duration used in previous studies on photodegradation under sunlight, from 15 to 70 days
249 (Moran et al., 2000; Vähätalo and Wetzel, 2004; Mostofa et al., 2007; Chupakova et al., 2018).
250 Dark control experiments were conducted also in duplicates, using sterilized glass tubes filled
251 with sterile 0.22 μm -filtered water, wrapped in Al foil and placed in the same outdoor pool as
252 the experiments. The headspace (approx. 20% of total reaction volume) was similar in
253 experimental and control reactors. The individual reactors were sterile sampled at the beginning
254 and after the 0, 2, 5, 8, 12, and 16 days of exposure. Each sampling sacrificed the entire reactor.
255 The Milli-Q blanks were collected and processed to monitor for any potential sample

256 contamination introduced by our filtration, incubation, handling and sampling procedures. The
257 organic carbon blanks of the filtrates did not exceed 0.2 mg/L.

258

259 *2.3. Analyses*

260 The temperature, pH, O₂ and specific conductivity in surface waters were measured in
261 the field. The dissolved CO₂ concentration in the studied bodies of water was measured in-situ
262 using submersible Vaissala Carbocap® GM70 handheld carbon dioxide meter with GMP222
263 probes (accuracy 1.5%; see Serikova et al. (2018, 2019) for methodological details). The
264 diffusional CO₂ flux was calculated using a wind-based model (Cole and Caraco, 1998) with k_{600}
265 $=2.07+0.215 \times u_{10}^{1.7}$, where u_{10} is the wind speed at 10 m height, following the approaches
266 developed for surface waters of peatlands (Zabelina et al., 2021).

267 The DOC and DIC were analyzed by high-temperature catalytic oxidation using a
268 Shimadzu® TOC-VCSN (uncertainty $\pm 2\%$, 0.1 mg L⁻¹ detection limit). DIC was measured after
269 sample acidification with HCl and DOC was analyzed in acidified samples after sparging it with
270 C-free air for 3 min at 100 mL min⁻¹ as non-purgable organic carbon (NPOC). Internationally
271 certified water samples (MISSISSIPPI-03 and Pérade-20) were used to check validity and
272 reproducibility of the analysis. Filtered sampled collected from photodegradation experiments
273 were acidified with ultrapure nitric acid and analyzed for major and TE following the procedures
274 employed by Geoscience and Environment Toulouse Laboratory for analyses of boreal humic
275 waters (Oleinikova et al., 2017, 2018).

276 The UV- and visual absorbance of water samples was measured using a 10 mm quartz
277 cuvette on a CARY-50 UV-vis spectrophotometer to assess the aromaticity of pore fluids via
278 specific UV absorbance (SUVA₂₅₄). In the filtrates, we measured optical density at 254 nm and
279 at selected wavelengths (365, 436, 470, and 665 nm) as well as the entire UV-visible spectrum.
280 The specific UV-absorbency (SUVA₂₅₄, L mg⁻¹ m⁻¹) and E₄₇₀:E₆₆₅ ratios are used as a proxy for

281 degree of condensation of aromatic groups of DOM, or humification (Chin et al., 1994; Weishaar
282 et al., 2003; Hur et al., 2006; Peacock et al., 2013). The ratio $E_{254}:E_{436}$ is useful for evaluation
283 of contributions of autochthonous (aquatic) DOM compared to terrestrial (soil) C (Hur et al., 2006;
284 Ilina et al., 2014). The ratio $E_{254}:E_{365}$ also allows approximating the mean molecular weight of
285 DOM (Hiriart-Baer et al., 2008; Berggren et al., 2007). For better visualization of the differences
286 in spectral parameters between experimental and control reactors, we calculated the difference
287 (ΔA) between the absorbance of the photo- or bio-reactor and that of the control reactor at each
288 sampling time.

289 Major cations, Si, P and ~40 TE were measured with a quadrupole ICP-MS (Agilent 7500
290 ce) using In and Re as internal standards. The international geo-standard SLRS-6 (Riverine Water
291 Reference Material for Trace Metals) was used to check validity and reproducibility of analyses.
292 Note that for both bio- and photodegradation experiments, ICP MS analyses were performed
293 over 16 days of incubation time.

294 To check for possible microbial development in biodegradation experiments, we
295 performed oligotrophic and eutrophic bacteria counts over the course of incubation, following
296 the standard methodology used in biodegradation experiments of peat waters (Stutter et al., 2013)
297 and also described previously (Shirokova et al., 2017b; Chupakova et al., 2018). Specifically,
298 active bacteria number count (colony forming units, CFU mL⁻¹) was performed using Petri dishes
299 inoculation (0.1 to 1.0 mL of lake water in three replicates) performed in a laminar hood box
300 immediately prior the experimental incubation start and upon each sampling. Samples were
301 inoculated on Nutrient Agar (5 g L⁻¹ beef extract, 5 g L⁻¹ gelatine peptone, 15 g L⁻¹ bacteriological
302 agar, pH=6.8±0.2 at 25 °C) to determine the total number of heterotrophic bacteria. Difco® agar
303 (granulated powder, Lot No 6290083) inoculation was used to assess the number of oligotrophic
304 bacteria. Inoculation of blanks was routinely performed to assure the absence of contamination
305 from external environments.

306 2.4. Data treatment

307 The bio- and photodegradable DOC and trace metals were calculated as percent loss
308 relative to control in similar fashion with other studies (Vonk et al., 2015; Chupakova et al.,
309 2018; Shirokova et al., 2017b, 2019). However, previous works in similar environmental
310 contexts of high-DOC humic waters demonstrated that the effects of DOC and element decrease
311 are rather low and often comparable to uncertainties of duplicates (Shirokova et al., 2019). To
312 assess the net effect of bio- or photodestruction during the experiment, we used the integral
313 values of concentration change, estimated as the difference between the experiment and the
314 control, while taking into account the standard deviation of replicates. For this, we first calculated
315 the mean of replicates at the i -th time of sampling for the experiment and the control of X
316 component ($^{mean}X_i$ and $^{control}X_i$, respectively). We next calculated the sum of mean concentration
317 of replicates and its standard deviation ($^{mean}X_i+SD_i$). Thus, we obtained 3 values characterizing
318 the bio- or photo-degradation process: 1) the change of concentration in the experimental reactor
319 (^{mean}S), 2) the change of concentration not linked to the studied process ($^{control}S$), and 3) the
320 maximal uncertainty of the concentration change in the reactor ($^{mean+SD}S$). This allowed
321 calculating, in percentages, the efficiency of bio or photodegradation of X component relative to
322 the control, taken into account relevant uncertainties as following:

323
$$X (\%) = 100 \times (|^{mean}X| - |^{control}X|) / |^{control}X| \quad (1)$$

324
$$SD (\%) = 100 \times (|^{mean+SD}X| - |^{mean}X|) / |^{control}X| \quad (2)$$

325 where X is biodegradable DOC or trace element (BDOC and BTE, respectively) or
326 photodegradable DOC and trace element (PDOC and PTE, respectively). The sign of X
327 designates either a decrease («-») or an increase («+») of solute concentration during the
328 experiment. We considered the decrease of concentration significant when $X (\%) > SD (\%)$. In
329 other cases, the change was non-systematic over the course of experiment or non-measurable
330 using the experimental technique employed in the present study.

331 The mean rate of bio- or photodegradation of X component (V_X) was calculated based on
332 the overall change (ΔX , in %) between the initial (X_0) and final value normalized to overall
333 duration of the experiment t (22 and 16 days for bio- and photodegradation, respectively):

$$334 \quad V_X = ((\Delta X/X_0) / t \quad (3)$$

335 The SD for rates of component change were calculated in a similar way.

336 The spectral differences between experimental and control reactors were presented as X-
337 Y-Z diagrams where X is elapsed time, Y is wavelength, and Z is ΔA . The data were plotted in
338 a Surfer software package using triangulation with a linear interpolation method. Statistical
339 treatment included the least squares method and the Pearson correlation, as the data were
340 normally distributed. All calculations were performed in STATISTICA ver. 10 (StatSoft
341 Inc.,Tulsa) at $p = 0.05$.

342

343 **3. Results**

344 *3.1. Field measured C concentration and calculated CO₂ fluxes*

345 The DOC concentration ([DOC]) ranged from 13 to 21 mg L⁻¹ in Lake Temnoe,
346 depending on depth and season. The CO₂ concentrations and fluxes increased from June to
347 October and varied from 99 to 220 $\mu\text{mol L}^{-1}$ and 32 to 71 mmol CO₂ m⁻² d⁻¹, respectively (**Table**
348 **1**). In Ilasskoe Bog hydrological continuum, the DOC decreased from 88 mg L⁻¹ in the peat soil
349 water to 38 mg L⁻¹ in the outlet stream. The DOC concentration was generally similar (within \pm
350 5 %) between 3, 0.8 (GFF), 0.45 and 0.22 μm pore size filtration of the initial sample, which is
351 in agreement with former size fractionation measurements for Arctic and subarctic systems
352 (Vasyukova et al., 2010; Pokrovsky et al., 2012, 2016, Shirokova et al., 2019). The waters of
353 Ilasskoe Bog continuum exhibited CO₂ supersaturation with respect to atmosphere (from 55 to
354 3300 $\mu\text{mol L}^{-1}$) and calculated CO₂ emission (diffusion) flux ranging from 22 mmol CO₂ m⁻² d⁻¹
355 in the peatland pool to 1600 mmol CO₂ m⁻² d⁻¹ in the piezometer (**Table 1**).

356 3.2. Biodegradation of DOM

357 3.2.1. DOC concentration evolution in the experiments

358 In the Temnoe Lake, the range of [DOC] change during 2-3 week incubation in the
359 experimental reactors did not exceed 2 mg L^{-1} and remained within $+0.5$ to -1.5 mg L^{-1} , which is
360 less than 10% of the initial DOC amount (**Fig. 2 A and Fig. S1** of the Supplement). The
361 biodegradable DOC was both season and depth dependent and ranged from 2 to 6 % (**Table 2**).
362 The integral 2-week rates of biodegradation (**Table 3, Fig. 3 A**) demonstrated the highest values
363 during autumn at depths of 0.5 m and 10 m and the lowest values during June at all depths. The
364 final 0-10 m water column- and season-averaged biodegradation rate in Lake Temnoe ranged
365 from 0.02 to $0.04 \text{ mg DOC L}^{-1} \text{ d}^{-1}$. Integral rates of bio-degradation in the 0-10 m layer
366 demonstrated an increase from May to October, over the entire open-water period (**Fig. 4 A**).

367 For Ilaskoe Bog, the BDOC was highest in the peatland pool ($4.9 \pm 1.4 \%$) and lowest
368 in the outlet stream ($3.1 \pm 2.4 \%$; **Fig. 2 A and Fig. S1**). The integral rate of DOC biodegradation
369 followed the order ‘piezometer >> stream > peatland pool’ and ranged from 0.03 to 0.17 mg C
370 $\text{L}^{-1} \text{ d}^{-1}$ (**Table 3, Fig. 3 A**).

371

372 3.2.2. Optical parameters of DOM

373 In Lake Temnoe, the SUVA_{254} remained relatively constant (4.2 to $4.6 \text{ L mg C}^{-1} \text{ m}^{-1}$)
374 across seasons and depths (**Table 1 B**). Over the course of biodegradation, the SUVA_{254} did not
375 change significantly (i.e., less than 0.2 units, which is comparable to the variability of duplicates;
376 **Fig. S2**). The ratio $E_{254}:E_{436}$, which is an indicator of humification, increased with incubation
377 time in Lake Temnoe waters; the magnitude of this increase across depth followed the order “0.5
378 m > 5 m > 10 m” (**Fig. S3**). The ratio E_{254}/E_{365} also increased over the course of biodegradation,
379 corresponding to an increase of mean molecular weight of DOM (Hiriart-Baer et al., 2008;
380 Berggren et al., 2007). The ratio E_{365}/E_{470} also demonstrated the strongest increase in surface

381 horizons and virtually no change in the deepest horizon (**Fig. S3**). An increase in the ratio
382 $E_{470}:E_{665}$ corresponds to a decrease in the degree of aromaticity (humification). An increase in
383 the ratio $E_{254}:E_{436}$ signifies a decrease in contribution of autochthonous (aquatic) DOM compared
384 to terrestrial (soil) C, whereas an increase in the $E_{254}:E_{365}$ ratio characterizes removal of low
385 molecular weights compounds.

386 In Ilasskoe Bog samples, the highest SUVA was observed in the water of the piezometer
387 and the lowest in the stream, but the evolution of this parameter in the course of biodegradation
388 was rather weak (**Fig. S3**). The $E_{254}:E_{365}$ and $E_{254}:E_{436}$ ratios increased with incubation time in
389 the piezometer and decreased with time in the stream (**Fig. S3**). The optical ratios ($E_{254}:E_{436}$,
390 $E_{365}:E_{470}$, $E_{470}:E_{665}$) increased in the peatland pool, suggesting an increase in the molecular
391 weight and an increase in the ratio of aromatic to aliphatic compounds.

392 Complete spectral differences between the experimental and control samples
393 demonstrated rather weak ($\Delta A \leq 0.04$) changes of spectral parameters, mostly detectable after
394 10-12 days of incubation (**Fig. S4**). These results were generally consistent with the discrete
395 spectral parameters presented above and demonstrated maximal effects in the piezometer and
396 bog outlet stream. In Lake Temnoe, the maximal impact of biodegradation on spectral parameters
397 was observed in June, at 0.5 m depth.

398

399 3.2.3. Bacterial number evolution during biodegradation experiments

400 The number of cultivable eutrophic bacteria (EB) sizably (ca., 2 orders of magnitude)
401 increased during biodegradation of Lake Temnoe waters. However, this evolution was not
402 systematic in the course of incubation; there was a pronounced decrease after 2 weeks of
403 exposure in June and August and rather stable concentration in waters of all horizons sampled in
404 October (**Fig. S5**). Such maxima in June and August might be linked to consumption of
405 substrate/nutrient limitations on bacterial growth. In Ilasskoe Bog continuum, the number of

406 eutrophic bacteria decreased by an order of magnitude in the peatland pool and piezometer while
407 it remained constant in the stream. The number of oligotrophic bacteria (OB) increased in waters
408 of all Lake Temnoe horizons by ca. 2 orders of magnitude in August and October and 1 order of
409 magnitude in June. In contrast, the OB number did not change or slightly decreased during
410 incubations of waters from Ilasskoe Bog continuum (**Fig. S5**).

411

412 3.2.4 Trace element behavior

413 During biodegradation experiments, a number of trace metals [Group 1] demonstrated a
414 significant ($X > SD$, Eqn. 1) decrease in concentration across the incubation period (**Table 2**):
415 Al, Ti, Fe, Co, Cu, Ba, Nb, light REE (LREE) and Pb (as illustrated for Fe in **Fig. 5**) as well as
416 Mn, V, and La (**Figs. S6, S7 and S8**, respectively). The most significant effects were observed
417 for Fe in the 0-5 m horizon of Lake Temnoe (9 to 18 % in June, 6 to 13.5 % in August and 8 to
418 9.5 % in October) and 14% in the peatland pool of Ilasskoe Bog. Overall, for most elements
419 except Fe and Mn, this increase was less pronounced than that of DOC; maximal effects were
420 achieved for Lake Temnoe in August and October (V, Mn, Co, Cu, Ni, Nb, Hf, Pb and Th) and
421 in June (Al and Ti). These elements are typically linked to DOM and Fe and present in the form
422 of organic- and organo-mineral colloids. Second group of major and trace elements did not
423 appreciably change their concentration ($< 2\%$ decrease): Li, B, Na, Mg, K, Ca, Si, Ge, As, Rb,
424 Sr, Mo, Sb, Mo and Ba. These elements are not linked to colloids of Fe(III) hydroxide and organic
425 matter. Finally, some elements [Group 3] exhibited unstable behavior without systematic change
426 in concentration during the exposure ($X < SD$, Eqns. 1-2): Cr, Zn, Cu, Sr, Cd, (Y, Zr), Cs, Tl and
427 U. These elements cannot be considered as significantly impacted by the biodegradation process
428 in Lake Temnoe water.

429 In the Ilasskoe Bog hydrological continuum, the most significant changes during
430 biodegradation were observed in the peatland pool and outlet stream. Elements strongly (> 5 -10

431 %; $X > S.D.$ in Eqn. 1) affected by biodegradation were organically / colloiddally complexed V,
432 Fe, Ni, Ga, Y, LREEs and Pb.

433

434 *3.3. Photodegradation of DOM*

435 3.3.1. DOC concentration evolution

436 Compared to biodegradation, photodegradation demonstrated much higher values of
437 PDOC and rates of reaction as well as higher variability among seasons and sites. In Lake
438 Temnoe, the PDOC was the highest in June and the lowest in October (**Fig. 2 B** and **Table 2**).
439 The maximal range of concentration change during 2-week period achieved 6-8 mg L⁻¹ (**Fig. S9**)
440 which was 10 to 20 % of the initial [DOC] values. The rates strongly decreased from May-June
441 to the end of summer – autumn. The depth integrated (0 to 10 m) rate of DOM photodegradation
442 in Lake Temnoe ranged from 0 in October to 0.2 mg C L⁻¹ d⁻¹ in June (**Table 3; Fig. 4 B**).

443 In the Ilaskoe Bog hydrological continuum during July, the photodegradation rate
444 followed the order “outlet stream > piezometer >> peatland pool” (**Fig. 3 B**), where integral rates
445 equaled to 0.27±0.04, 0.33±0.07, and 0±0.05 mg C L⁻¹ d⁻¹, respectively (**Table 3**).

446

447 3.3.2. Optical parameters of DOM

448 Similar to the DOC concentration, the optical parameters of DOM more strongly evolved
449 over the course of photodegradation compared to the biodegradation experiments. In the Temnoe
450 Lake, the strongest decrease in SUVA₂₅₄ was observed in the waters of all horizons in June. This
451 decrease was less pronounced in October (**Fig. S10**). The E₂₅₄:E₃₆₅ ratio demonstrated a sizable
452 increase in June, with much weaker increase in October. The E₂₅₄:E₄₃₆ ratio strongly decreased
453 with exposure time throughout all seasons (10 m depth) and only in June in the surface horizons
454 (**Fig. S11**). An increase in the ratio E₂₅₄:E₃₆₅ over the course of photodegradation corresponded
455 to an increase in mean molecular weight of DOM. The ratios E₃₆₅:E₄₇₀ and E₄₇₀:E₆₆₅ decreased

456 in all experiments with the Temnoe Lake waters (**Fig. S11**), suggesting a decrease in the degree
457 of humification (Battin, 1998) and a decrease in the ratio of aromatic to aliphatic moieties.

458 The SUVA₂₅₄ in Ilasskoe Bog waters remained stable during photodegradation of stream
459 waters and piezometer and strongly decreased in the peatland pool (**Fig. S10**). The E₂₅₄:E₄₃₆ ratio
460 strongly increased in the peatland pool and exhibited a decrease in stream waters and piezometer,
461 whereas the E₃₆₅:E₄₇₀ ratio systematically decreased in all photodegradation experiments with
462 the Ilasskoe Bog continuum (**Fig. S11**). Finally, the E₄₇₀:E₆₆₅ ratio exhibited sizable decrease, in
463 the order 'stream >> pool ≥ piezometer'. The total spectral differences between experimental and
464 control reactors were mostly pronounced in stratified forest lake waters in June ($\Delta A = -0.4$ to -
465 0.4) and in the bog continuum in July, where effects were strongest in the piezometer and outlet
466 stream waters (ΔA parameter as high as - 0.4 (**Fig. S12**).

467

468 3.3.3. TE in photodegradation experiments

469 The elements affected by photodegradation also formed three groups similar to those
470 impacted by biodegradation. Concentrations of Al, Fe, trivalent and tetravalent hydrolysates (Ti,
471 Ga, Zr, Y, LREE and Th) and Nb of [Group 1] significantly (> 2 %; $p < 0.05$) decreased during
472 photolysis as illustrated for Fe in **Fig. 6**, and for Ti and Zr in **Figs. S13** and **S14**, respectively.
473 The decrease of Fe was mostly pronounced in Lake Temnoe water from 10 m depth, whereas
474 that of Ti and Zr was detectable for all horizons and seasons except in October. For the Ilasskoe
475 Bog continuum, there was no systematic change in Fe concentration, whereas concentrations of
476 Ti and Zr systematically decreased over the course of sunlight exposure (**Figs. S13, S14**). Alkali
477 (Li, Rb), alkaline-earth metals (Mg, Ca, Sr, Ba), Si and oxyanions (As, Mo, Sb) of [Group 2]
478 were weakly (< 2 %) affected by photolysis. Finally, the remaining trace elements of [Group 3]
479 did not exhibit any systematic evolution of concentration during exposure to sunlight, or these
480 changes were inferior to the uncertainties of replicates ($X < S.D.$ in Eqn. 1).

481 We found that, unlike for DOC, the magnitude of trace element concentration decrease
482 during photodegradation was generally lower than that of biodegradation experiments. Overall,
483 the strongest effects were observed for Ti (3 to 9% in Lake Temnoe; 20% in Ilasskoe Bog), Ga
484 (6 to 14%), Zr (14-17% in Lake Temnoe), Nb (8 to 13%) and Th (8 to 19% in the Temnoe Lake
485 and up to 50% in the Ilasskoe Bog). These effects were mostly pronounced in the Temnoe Lake
486 in June and August and in peatland pool of the Ilasskoe Bog (July).

487

488 **4. Discussion**

489 *4.1. Comparison between biodegradation and photolysis*

490 The impact of season on the biodegradable DOC could be tested only for Lake Temnoe
491 because it was sampled during the 3 main hydrological periods. The maximal biodegradation of
492 the lake water was observed during autumn, when large amount of labile fresh soil OM and plant
493 litter were delivered to the lake from the watershed via surface runoff. The water temperature
494 seems to be of secondary importance for the intensity and rate of DOM biodegradation. This is
495 also confirmed by lack of statistically significant (at $p < 0.05$) correlation between water
496 temperature and BDOC parameters (overall magnitude and rate). It is worth noting that the
497 seasonal pattern of BDOC in the humic lake quantified in this study (**Fig. 4 A**) contrasted with
498 previous works on biodegradation of large Arctic streams and rivers whose BDOC decreased as
499 the Arctic summer progressed (Vonk et al., 2015). Presumably, the input of fresh plant litter from
500 the forested watershed of Lake Temnoe provided elevated biodegradation in the water column at
501 the end of the open water season. Another reason could be due to lake overturn in October and
502 exposure of deep, partially autochthonous, and thus biodegradable, DOM to the surface horizons.
503 A supply of limiting nutrients (N and P) to the upper 0-10 m layer during lake overturn could
504 also promote such biodegradation in October.

505 The highest biodegradation rates in the uppermost sections of the bog hydrological
506 continuum (piezometer, **Fig. 3 A**) are consistent with recent findings on organic-rich waters of
507 permafrost peatlands (Shirokova et al., 2019; Payandi-Rolland et al., 2020) and earlier results on
508 headwaters, small streams and soil leachates (Roehm et al., 2009; Ilina et al., 2014; Mann et al.,
509 2014, 2015; Larouche et al., 2015; Spencer et al., 2015; Vonk et al., 2015; Moody et al., 2013;
510 Pickard et al., 2017; Dean et al., 2019). This could be due to the very short water residence time
511 and freshly leached DOM in these water objects (i.e., Mann et al., 2012; Abbott et al., 2014;
512 Payandi-Rolland et al., 2020), given that bioavailable DOM components leached from plant litter
513 are rapidly utilized (Textor et al., 2018). At the same time, overly low BDOC (2-8 %) values,
514 regardless of depth and season in humic lake and across the hydrological continuum of the bog
515 (**Fig. 2 A**), are supportive of previous results for permafrost peatlands from the neighboring
516 region (Shirokova et al., 2019). A general path for DOM spectral properties modification over
517 the course of biodegradation consisted of an increase in aromaticity of DOM due to preferential
518 uptake of non-humic low molecular weight (LMW) compounds. However, this was not
519 accompanied by a sizable increase in SUVA (**Fig. S2**). Presumably, the proportion of these
520 compounds in the overall DOC level was quite low and could not impact SUVA evolution.
521 Globally, the evolution of optical ratios was consistent with bacterial consumption of aliphatic
522 LMW compounds and an increase in the overall aromaticity of DOM.

523 Concerning the seasonal variation of photodegradation in the deep humic lake, maximal
524 effects were observed in June. These effects likely occurred due to fresh terrestrial organic matter
525 that was leached from the watershed and then efficiently processed during Arctic summer. It
526 should be noted that labile phenolic, carbohydrates, N-containing bases and smaller molecular
527 weight compounds are abundant in litter leachates produced during initial decay stages (Kiikkilä
528 et al., 2011, 2012, 2013; Hensgens et al., 2021). By July, most of the biodegradable DOM was
529 already removed, and in October, the effects were much lower. Therefore, photolabile DOM is

530 delivered from the forested watershed to the lake essentially during surface flux, at high water
531 flow. It is then quickly removed from the water column, which was especially seen in the 0.5 and
532 5 m horizons of Lake Temnoe. Although labile organic matter from litter fall was also delivered
533 during autumn rain season, presumably, during this period, the conditions for photolysis (low
534 temperature, short daytime period and insufficient light) were not as favorable as those in June
535 or August.

536 Photodegradation of waters from the Ilasskoe Bog continuum demonstrated maximal
537 rates in the piezometer (**Fig. 3 B**). During photolysis of humic water, a decrease in optical ratios
538 ($E_{365}:E_{470}$; $E_{470}:E_{665}$) clearly indicated preferential degradation of humic aromatic compounds.
539 The strong effect of photodegradation on DOM optical properties in the 650-500 nm region may
540 be linked to decomposition of complex DOM into smaller molecules, whereas a decrease of
541 absorbance in the 230-400 nm region (**Fig. S12**) indicates degradation of aromatic compounds,
542 progressively increasing over insolation time. A recent study of DOM photolysis in humic-rich
543 forested streams demonstrated that high aromatic material was photochemically converted into
544 smaller non-fluorescent molecules (Wilske et al., 2020).

545 Results obtained on the more important role of photodegradation over biodegradation are
546 generally consistent with earlier reports on the dominance of photolysis for DOM processing in
547 Arctic waters within North America (Cory et al., 2014; Ward et al., 2017), the Canadian
548 temperate zone (Winter et al., 2007; Porcal et al., 2013, 2014, 2015), and Swedish headwater
549 catchments (Köhler et al., 2002). According to former results for Scandinavian surface waters,
550 the main impact of DOM photolysis is reflected by a decrease in the proportion of aromatic
551 (colored) DOC and a rather small ($\leq 10\%$) change in bulk DOC concentration (Groeneveld et
552 al., 2016; Koehler et al., 2014), Canada (Laurion and Mladenov, 2013; Gareis and Lesack, 2018)
553 and NW Russia (Oleinikova et al., 2017; Chupakova et al., 2018).

554 As a further perspective of this work, one has to consider biodegradation of photolytically
555 altered DOM given that photo-oxidation is known to transform molecular structures into more
556 bioavailable forms (e.g., Cory and Kling, 2018; Sulzberger et al., 2019) thereby stimulating
557 microbial growth under sunlight, as is known for other Arctic and subarctic settings (i.e.,
558 Drozodova et al., 2020; Laurion et al., 2020).

559

560 *4.2. Possible impact of microbial and photolytic processing on CO₂ emissions from* 561 *water surfaces*

562 A broad importance of DOM bio- and photodegradation dynamics is that these processes
563 can contribute to CO₂ emissions from water surfaces thereby directly controlling the C cycling
564 between the land and the atmosphere (Lapierre et al., 2013; Tranvik et al., 2009; Cory et al.,
565 2014, 2018). In this study, we attempted to relate, for the first time for several diverse aquatic
566 systems across seasons, experimentally measured rates of DOM degradation to in-situ measured
567 CO₂ emissions. The integral rates of DOM bioprocessing in the water column of Lake Temnoe
568 (**Table 3, Fig. 4 A**) allow quantifying the potential contribution of biodegradation to CO₂
569 production and emission. Assuming all biodegraded DOM is transformed into CO₂ and there is
570 no biomass increase or sedimentation, a 1 m water layer of the lake can emit 1.7 mmol CO₂ m⁻²
571 d⁻¹ in June and 3.3 mmol CO₂ m⁻² d⁻¹ in October. Therefore, integral flux from 10 m deep water
572 layer amounts to 17 – 33 mmol CO₂ m⁻² d⁻¹ across the seasons. These values are comparable to
573 typical values of CO₂ evasion from the surface of this lake during different seasons (30-70 mmol
574 CO₂ m⁻² d⁻¹; **Table 1 B**). For surface waters of Ilasskoe Bog, maximal CO₂ production due to
575 DOM biomineralization alone (**Table 3**) ranged from 5.0 mmol CO₂ m⁻² d⁻¹ for the peatland pool
576 (2 m deep) to 2.5 mmol CO₂ m⁻² d⁻¹ for the outlet stream (0.5 m deep). However, in summer, the
577 peatland pool and stream emitted 23 and 150 mmol CO₂ m⁻² d⁻¹ (**Table 1 A**) which could not be
578 sustained by DOM biodegradation.

579 The addition of photodegradation (assuming a photic layer depth of 3.5 m) to DOM
580 bioprocessing in the water column of the Temnoe Lake during open water season can further
581 increase potential CO₂ production in the water column. For the case of Ilasskoe Bog waters, the
582 addition of photolytic degradation increases projected CO₂ emission from the outlet stream by a
583 factor of 5, which is still below the actual CO₂ flux, whereas DOM photolysis has no impact on
584 CO₂ emissions from the peatland pool. Note that, although the depth of sunlight processing in
585 boreal waters is typically 1-0.8 m (Vähätalo et al., 2000; Koehler et al., 2014), a more recent
586 study concluded that direct photomineralization of DOM in Arctic humic ponds is limited to the
587 first centimeters of the water column (Mazoyer et al., 2022). Furthermore, in typical DOM-rich
588 Arctic waters, only half of sunlight-associated DOC losses is converted into CO₂ and the rest
589 may be turned into particles through photoflocculation (e.g., Mazoyer et al., 2022). Therefore,
590 despite a faster photodegradation rate compared to biodegradation, due to the shallow photic
591 layer in humic waters, the biodegradation may provide the largest impact on CO₂ emission from
592 the water column of boreal waters.

593 At the same time, our assumption that all CO₂ in lake water is produced by bio- or
594 photodegradation of DOM might not be warranted because there are multiple sources of CO₂ in
595 the lake waters, which were not assessed in the present study. These including but not limited to:
596 particulate organic matter bio- and photodegradation, whose importance can strongly exceed that
597 of DOC (e.g., Attermeyer et al., 2018; Keskitalo et al., 2022), sediment respiration, plankton and
598 periphyton diel photosynthetic cycle, underground water discharge at the lake bottom, and
599 delivery of DOC and CO₂-rich waters via lateral surface and shallow subsurface influx. Given
600 that the contribution of each CO₂ source can vary among different water bodies and across
601 seasons, the assessment of DOM bio- and photodegradation contribution to overall CO₂ flux in
602 this study should be considered as highly conservative.

603

604 *4.3. Impact of DOM bio- and photo transformation on trace element pattern*

605 In this study we hypothesized the following link between DOC and TE: in humic surface
606 waters of peatlands, most TE, which include divalent transition metals (Cu, Ni, Co, Zn, Mn),
607 toxicants (Be, Cr, Cd, Pb), trivalent and tetravalent hydrolysates (Al, Ga, Y, REE, Ti, Zr, Hf,
608 Th), with an exception of some alkalis and oxyanions, are strongly (> 80%) associated to DOM
609 in the form of organic, organo-ferric and organo-aluminium colloids (Pokrovsky et al., 2012,
610 2016). As a result, any DOM transformation processes, be it bio- or photo-degradation, may
611 directly affect the concentration pattern of TE. Specifically, the DOM removal via photo- or bio-
612 degradation should change the speciation of those elements, that are strongly bound to DOM
613 such as divalent transition metals, or incorporated into organo-mineral (Fe, Al) colloids, such as
614 trivalent and tetravalent hydrolysates (TE^{3+} , TE^{4+}). The former might either remain in solution
615 (during photodegradation), hence not modifying their total dissolved concentration, or being
616 taken up by growing bacteria during bio-degradation. The latter (TE^{3+} , TE^{4+}) are capable of co-
617 precipitating with Fe and Al hydroxides, especially during photodegradation (i.e., Kopacek et al.,
618 2005, 2006), hence being sizably removed from the aqueous solution. From the other hand, some
619 TE are known to be photosensitive (Mn, Fe), toxic (Al, Cu, As, Cd, Pb), or potentially limiting
620 micronutrients (Zn, Co, Ni, Mo) for the bacteria and therefore they are capable affecting the
621 overall rate of photo- or bio-degradation.

622 However, contrary to our expectations, among all major and trace elements measured in
623 the experiments, only trivalent and tetravalent hydrolysates (TE^{3+} , TE^{4+}) were impacted by both
624 photo- and biodegradation. It is known that these elements are essentially present in the form of
625 large molecular size, highly polymerized and presumably aromatic, organo-Fe/Al colloids in
626 humic boreal/subarctic lakes (Pokrovsky et al., 2012, 2016), rivers (Krickov et al., 2019;
627 Pokrovsky et al., 2010), and soil porewaters (Pokrovsky et al., 2005; Raudina et al., 2021).
628 Therefore, insoluble TE^{3+} and TE^{4+} generally followed the removal of Fe(III) in the form of

629 particulate Fe hydroxides, after breaking the Fe-DOM bonds that stabilized colloidal Fe(III)
630 hydroxides. This destabilization and Fe hydroxide particle formation is known to occur either via
631 biodegradation (i.e., Oleinikova et al., 2018) or photolysis (Kopacek et al., 2005, 2006;
632 Oleinikova et al., 2017; Chupakova et al., 2018). At the same time, some micronutrients (V, Mn,
633 Co, Cu and Ba) were affected solely by biodegradation. This can reflect uptake of these metals
634 by growing bacterial cells, as is known from laboratory experiments with pure cultures of
635 heterotrophic bacteria (Shirokova et al., 2017a).

636 Note that the effects of bio- and photodegradation were more pronounced for light REE
637 (LREE) compared to heavy REE (HREE). This result is consistent with the fact that LREE have
638 stronger association with Fe hydroxide compared to organic complexes, as known from general
639 chemical considerations and laboratory experiments (i.e., Bau, 1999) and evidenced in various
640 boreal and subarctic settings (Pokrovsky et al., 2016; Krickov et al., 2019). Given that the main
641 effect of both photolysis and biodegradation of DOM in humic Fe(III)-rich surface waters is
642 coagulation of dissolved Fe(III) in the form of Fe oxy(hydr)oxides, the LREE are removed from
643 solution. This removal occurs in the form of adsorbed complexes or coprecipitated with Fe
644 oxy(hydr)oxides, while HREE remain in the form of strong aqueous complexes.

645 In former studies of photo- and biodegradation of surface waters from permafrost
646 peatlands, only a few nutrients (P, Fe, Zn and V) and insoluble low mobility trace metals (Ti, Zr,
647 Nb and Th) demonstrated a decrease in concentration (Shirokova et al., 2019). This list of
648 elements is generally consistent with that established in the present study of humic subarctic
649 lakes of the non-permafrost zone, except P and Zn which did not exhibit sizable removal in our
650 experiments. It is possible that a high proportion of low molecular weight $LMW_{<1\text{ kDa}}$ (and thus,
651 potentially bioavailable) forms of macro- and micronutrients, such as P and Zn, in the permafrost
652 ice (i.e., Kuzmina et al., 2023) can be delivered to the lake and river via suprapermafrost flow
653 (Raudina et al., 2018, 2021). This led to elevated bioavailability of these elements in permafrost

654 surface waters reported in previous works, as compared to permafrost-free boreal settings of this
655 study.

656

657 **Conclusions**

658 Seasonally resolved bio- and photo-degradability of DOM in a deep stratified lake and
659 summer measurements from a peat bog's hydrological continuum within the boreal zone
660 demonstrated that the subsurface and deep horizons of these stratified waters are mostly sensitive
661 to sunlight impact, and that maximal effects of photodegradation occurred in June, during strong
662 insolation. In contrast, the biodegradation of DOM from the humic lake was mostly pronounced
663 during October, when fresh leachates of forest litter were exported from the watershed. Insoluble,
664 low-mobility trace metals such as trivalent and tetravalent hydrolysates were affected by both
665 bio- and photodegradation, as they are associated with coagulating Fe(III) oxyhydroxides.

666 A broad implication of obtained results is that, although DOM photodegradation rates
667 were sizably higher compared to those of biodegradation, the rather thin photic layer in humic
668 waters does not allow for significant contribution of photolysis in overall CO₂ emission from
669 lake and bog surfaces. Further work is needed on biodegradation of photolytically altered DOM
670 given that photo-oxidation is known to transform molecular structures into more bioavailable
671 forms. The high seasonal dynamics and spatial variability in both photo- and biodegradability of
672 DOM and related trace elements of humic surface waters in the boreal zone encountered in this
673 study suggest the need for studying these processes during “shoulder seasons” (early spring and
674 late autumn), the periods of maximal photo- and biodegradation, respectively. These efforts
675 should be focused on the most dynamic components such as small streams and subsurface waters,
676 which demonstrated the highest rates of both photo- and biodegradation.

677

678

679 **Acknowledgements**

680 This work was supported by RSF grant No 22-17-00253. LS and OP were also supported
681 by project PEACE of PEPR FairCarboN ANR-22-PEXF-0011. OP is grateful for partial support
682 from the TSU Development Programme Priority-2030.

683

684 **Assets:** All the data obtained in this work are presented in Supplementary Information file.

685

686 **Authors contribution.**

687 AVC and OP designed the study and wrote the paper; AC, NN and SB performed sampling,
688 analysis and their interpretation; LS performed bacterial number assessment and DOC results
689 interpretation; AVC, TV and OP provided analyses of literature data.

690

691 **Competing interests.**

692 The authors declare that they have no conflict of interest.

693

694

695

696 **References**

697 Abbott, B. W., Larouche, J. R., Jones, J. B., Bowden, W. B., and Balsler, A. W.: Elevated
698 dissolved organic carbon biodegradability from thawing and collapsing permafrost, J.
699 Geophys. Res., 119, 2049–2063, <https://doi.org/10.1002/2014JG002678>, 2014.

700 Amado, A. M., Cotner, J. B., Cory, R. M., Edhlund, B. L., and McNeill, K.: Disentangling the
701 interactions between photochemical and bacterial degradation of dissolved organic matter:
702 amino acids play a central role, Microb. Ecol., 69(3), 554-566, doi: 10.1007/s00248-014-
703 0512-4, 2014.

704 Amaral, V., Ortega, T., Romera-Castillo, C., and Forja, J.: Linkages between greenhouse gases
705 (CO₂, CH₄, and N₂O) and dissolved organic matter composition in a shallow estuary, Sci.
706 Total Environ. 788, Art No 147863, <https://doi.org/10.1016/j.scitotenv.2021.147863>, 2021.

707 Andersson, M. G. I., Catalán, N., Rahman, Z., Tranvik, L. J., and Lindström, E. S.: Effects of
708 sterilization on dissolved organic carbon (DOC) composition and bacterial utilization of
709 DOC from lakes, Aquat. Microb. Ecol., 82, 199-208, <http://dx.doi.org/10.3354/ame01890>,
710 2018.

711 Ask, J., Karlsson, J., and Jansson, M.: Net ecosystem production in clear-water and brown-water
712 lakes, Glob. Biogeochem. Cycles, 26, GB1017, doi:10.1029/2010GB003951, 2012.

713 Attermeyer, K., Catalán, N., Einarsdottir, K., Freixa, A., Groeneveld, M., Hawkes, J. A., et al.:
714 Organic carbon processing during transport through boreal inland waters: Particles as
715 important sites, J. Geophys. Res.: Biogeosciences, 123(8), 2412–2428.
716 <https://doi.org/10.1029/2018jg004500>, 2018.

717 Bau, M.: Scavenging of dissolved yttrium and rare earths by precipitating iron oxyhydroxide:
718 experimental evidence for Ce oxidation, Y-Ho fractionation, and lanthanide tetrad effect,
719 Geochim. Cosmochim. Ac., 63, 67–77, doi: 10.1016/S0016-7037(99)00014-9, 1999.

720 Battin T.J. Dissolved organic materials and its optical properties in a blackwater tributary of the
721 upper Orinoco River, Venezuela, *Organic Geochemistry*, 28, 561-569,
722 [https://doi.org/10.1016/S0146-6380\(98\)00028-X](https://doi.org/10.1016/S0146-6380(98)00028-X), 1998.

723 Begum, M. S., Park, J.-H., Yang, L., Shin, K. H., and Hur, J.: Optical and molecular indices of
724 dissolved organic matter for estimating biodegradability and resulting carbon dioxide
725 production in inland waters: A review. *Water Research*, Art No 119362,
726 <https://doi.org/10.1016/j.watres.2022.119362>, 2022.

727 Berggren, M., Laudon, H., and Jansson, M.: Landscape regulation of bacterial growth efficiency
728 in boreal freshwaters, *Global Biogeochem. Cy.*, 21, GB4002.
729 <http://dx.doi.org/10.1029/2006GB002844>, 2007.

730 Berggren, M., Laudon, H., Haei, M., Ström, L., and Jansson, M.: Efficient aquatic bacterial
731 metabolism of dissolved low-molecular-weight compounds from terrestrial sources, *ISME*
732 *J.*, 4, 408-416, <https://doi.org/10.1038/ismej.2009.120>, 2010.

733 Borges, A., Darchambeau, F., Teodoru, C. et al. : Globally significant greenhouse-gas emissions
734 from African inland waters, *Nature Geosci.*, 8, 637–642. <https://doi.org/10.1038/ngeo2486>,
735 2015.

736 Chaudhary, N., Westermann, S., Lamba, S., et al.: Modelling past and future peatland
737 carbon dynamics across the pan- Arctic, *Glob. Change Biol.*, 26, 4119-4133, doi:
738 10.1111/gcb.15099, 2020.

739 Chin, Y.-P., Aiken, G., and O'Loughlin, E.: Molecular weight, polydispersity, and spectroscopic
740 properties of aquatic humic substances, *Environ. Sci. Technol.*, 28, 1853-1858,
741 <https://pubs.acs.org/doi/10.1021/es00060a015>, 1994.

742 Chupakov, A., Ershova, A., Moreva, O. Yu, Shirokova, L. S., Zabelina, S. A., Vorobieva, T. Ya.,
743 Klimov, S. I., Brovkon N., Pokrovsky, O.S.: Seasonal dynamics of dissolved carbon in
744 contrasting stratified lakes of the subarctic, *Boreal Environ. Res.*, 22, 213–230,
745 <https://www.borenav.net/BER/archive/pdfs/ber22/ber22-213-230.pdf>, 2017.

746 Chupakova, A. A., Chupakov, A. V., Neverova, N. V., Shirokova, L. S., and Pokrovsky, O. S.:
747 Photodegradation of river dissolved organic matter and trace metals in the largest European
748 Arctic estuary, *Sci. Total Environ.*, 622–623, 1343–1352,
749 <http://dx.doi.org/10.1016/j.scitotenv.2017.12.030>, 2018.

750 Cole, J. J. and Caraco, N.: Atmospheric exchange of carbon dioxide in a low-wind oligotrophic
751 lake measured by the addition of SF₆, *Limnol. Oceanogr.*, 43, 647–656,
752 <https://doi.org/10.4319/lo.1998.43.4.0647>, 1998.

753 Cole, J. J., Prairie, Y. T., Caraco, N. F., McDowell, W. H., Tranvik, L. J., Striegl, R. G., Duarte,
754 C. M., Kortelainen, P., Downing, J. A., Middelburg, J. J., and Melack, J.: Plumbing the
755 global carbon cycle: Integrating inland waters into the terrestrial carbon budget, *Ecosystems*,
756 10, 172–185, <https://doi.org/10.1007/s10021-006-9013-8>, 2007.

757 Cory, R. M., Ward, C. P., Crump, B. C., and Kling, G. W.: Sunlight controls water column
758 processing of carbon in arctic fresh waters, *Science*, 345, 925-928,
759 <https://doi.org/10.1126/science.1253119>, 2014.

760 Cory, R. M., and Kling, G. W.: Interactions between sunlight and microorganisms influence
761 dissolved organic matter degradation along the aquatic continuum, *Limnol. Oceanogr. Lett.*,
762 3, 102–116, <https://doi.org/10.1002/lo2.10060>, 2018.

763 Dean, J. F., van Hal, J. R., Dolman, A. J., Aerts, R., and Weedon, J. T.: Filtration artefacts in
764 bacterial community composition can affect the outcome of dissolved organic matter
765 biolability assays, *Biogeosciences*, 15, 7141-7154, [https://doi.org/10.5194/bg-15-7141-](https://doi.org/10.5194/bg-15-7141-2018)
766 2018, 2018.

767 Dean, J. F., Garnett, M. H., Spyrakos, E., Billett, M. F.: The potential hidden age of dissolved
768 organic carbon exported by peatland streams, *J. Geophys. Res.: Biogeosciences*,
769 124, 328–341, <http://dx.doi.org/10.1029/2018JG004650>, 2019.

770 Don, A., and Kalbitz, K.: Amount and degradability of dissolved organic carbon from foliar litter
771 at different decomposition stages, *Soil Biol. Biochem.*, 37, 2171-2179,
772 <http://dx.doi.org/10.1016/j.soilbio.2005.03.019>, 2005.

773 Drozdova, O. Y., Aleshina, A. R., Tikhonov, V. V., Lapitskiy, S. A., and Pokrovsky, O. S.:
774 Coagulation of organo-mineral colloids and formation of bioavailable low molecular weight
775 organic complexes in boreal humic river water under UV-irradiation, *Chemosphere*, 250,
776 Art No 126216, doi.org/10.1016/j.chemosphere.2020.126216, 2020.

777 Gareis, J. A. L., and Lesack, L. F. W.: Photodegraded dissolved organic matter from peak
778 freshet river discharge as a substrate for bacterial production in a lake-rich great Arctic delta,
779 *Arctic Science*, 4(4), 557-583, <http://dx.doi.org/10.1139/AS-2017-0055>, 2018.

780 Groeneveld, M., Tranvik, L., Natchimuthu, S., and Koehler, B.: Photochemical mineralisation in
781 a boreal brown water lake: considerable temporal variability and minor contribution to
782 carbon dioxide production, *Biogeoscience*, 13, 3931-3943, [https://doi.org/10.5194/bg-13-](https://doi.org/10.5194/bg-13-3931-2016)
783 [3931-2016](https://doi.org/10.5194/bg-13-3931-2016), 2016.

784 Harris, L. I., Richardson, K., Bona, K. A., Davidson, S. J., Finkelstein, S. A., Garneau, M.,
785 McLaughlin, J., Nwaishi, F., Olefeldt, D., Packalen, M., Roulet, N. T., Southee, F. M.,
786 Strack, M., Webster, K. L., Wilkinson, S. L., and Ray, J. C.: The essential carbon service
787 provided by northern peatlands, *Front. Ecol. Environ.*, 20, 222–230,
788 <https://doi.org/10.1002/fee.2437>, 2022.

789 Henggens, G., Lechtenfeld, O. J., Guillemette, F., Laudon, H., Berggren, M.: Impacts of litter
790 decay on organic leachate composition and reactivity, *Biogeochemistry* 154, 99-117,
791 <https://link.springer.com/article/10.1007/s10533-021-00799-3>, 2021.

792 Hirriart-Baer, V.P., Diep, N., and Smith, R.E.H.: Dissolved organic matter in the Great Lakes: role
793 and nature of allochthonous material, *J. Great Lakes Res.* 34, 383–394,
794 [https://doi.org/10.3394/0380-1330\(2008\)34\[383:DOMITG\]2.0.CO;2](https://doi.org/10.3394/0380-1330(2008)34[383:DOMITG]2.0.CO;2), 2008.

795 Hur, J., Williams, M. A., and Schlautman, M. A.: Evaluating spectroscopic and chromatographic
796 techniques to resolve dissolved organic matter via end member mixing analysis, *Chemosphere*,
797 63, 387-402, <https://doi.org/10.1016/j.chemosphere.2005.08.069>, 2006.

798 Ilina, S. M., Drozdova, O. Yu., Lapitskiy, S. A., Alekhin, Yu. V., Demin, V. V., Zavgorodnaya, Yu.
799 A., Shirokova, L. S., Viers, J., and Pokrovsky, O. S.: Size fractionation and optical properties
800 of dissolved organic matter in the continuum soil solution-bog-river and terminal lake of a
801 boreal watershed, *Org. Geochem.*, 66, 14–24,
802 <http://dx.doi.org/10.1016/j.orggeochem.2013.10.008>, 2014.

803 Kalbitz, K., Schmerwitz, J., Schwesig, D., and Matzner, E.: Biodegradation of soil-derived
804 dissolved organic matter as related to its properties, *Geoderma* 113, 273-291,
805 [https://doi.org/10.1016/S0016-7061\(02\)00365-8](https://doi.org/10.1016/S0016-7061(02)00365-8), 2003.

806 Karlsson, J., Serikova, S., Rocher-Ros, G., Denfeld, B., Vorobyev, S. N., Pokrovsky, O. S.:
807 Carbon emission from Western Siberian inland waters, *Nature Comm.*, 12, 825,
808 <https://doi.org/10.1038/s41467-021-21054-1>, 2021.

809 Kawahigashi, M., Kaiser, L., Kalbitz, K., Rodionov, A., and Guggenberger, G.: Dissolved
810 organic matter in small streams along a gradient from discontinuous to continuous
811 permafrost. *Global Change Biol.* 10, 1576-1586, [https://doi.org/10.1111/j.1365-](https://doi.org/10.1111/j.1365-2486.2004.00827.x)
812 [2486.2004.00827.x](https://doi.org/10.1111/j.1365-2486.2004.00827.x), 2004.

813 Keskitalo, K.H., Bröder, L., Jong, D., Zimov, N., Davydova, A., Davydov, S., Tesi, T., Mann, P.
814 J., Haghipour, N., Eglinton, T. I., and Vonk, J. E.: Seasonal variability in particulate organic

815 carbon degradation in the Kolyma River, Siberia. *Environmental Research Letters*, 17(3),
816 Art No 034007. DOI 10.1088/1748-9326/ac4f8d, 2022.

817 Kiikkilä, O., Kitunen, V., and Smolander, A.: Properties of dissolved organic matter derived
818 from silver birch and Norway spruce stands: Degradability combined with chemical
819 characteristics, *Soil Biol. Biochem.* 43, 421-430,
820 <http://dx.doi.org/10.1016/j.soilbio.2010.11.011>, 2011.

821 Kiikkilä, O., Kitunen, V., Spetz, P., and Smolander, A.: Characterization of dissolved organic
822 matter in decomposing Norway spruce and silver birch litter, *European J Soil Sci* 63, 476-
823 486, <http://dx.doi.org/10.1111/j.1365-2389.2012.01457.x>, 2012.

824 Kiikkilä, O., Smolander, A., and Kitunen, V.: Degradability, molecular weight and adsorption
825 properties of dissolved organic carbon and nitrogen leached from different types of
826 decomposing litter, *Plant Soil* 373, 787-798, <https://doi.org/10.1016/j.femsec.2004.08.011>,
827 2013.

828 Koehler, B., Landelius, T., Weyhenmeyer, G. A., Machida, N., and Tranvik, L.J.: Sunlight-
829 induced carbon dioxide emissions from inland waters, *Global Biogeochem. Cycles*, 28, 696-
830 711, <https://doi.org/10.1002/2014GB004850>, 2014.

831 Köhler, S., Buffam, I., Jonsson, A., and Bishop, K.: Photochemical and microbial processing of
832 stream and soil water dissolved organic matter in a boreal forested catchment in northern
833 Sweden, *Aquat. Sci.*, 64, 269-281, <http://dx.doi.org/10.1007/s00027-002-8071-z>, 2002.

834 Kopáček, J., Klementova, S., and Norton S. A.: Photochemical production of ionic and
835 particulate aluminum and iron in lakes, *Environ. Sci. Technol.*, 39, 3656-3662,
836 <https://pubs.acs.org/doi/10.1021/es048101a>, 2005.

837 Kopáček, J., Marešová, M., Norton, S. A., Porcal, P., and Veselý, J.: Photochemical source of
838 metals for sediments, *Environ. Sci. Technol.*, 40(14), 4455-4459.
839 <https://doi.org/10.1021/es0600532>, 2006.

840 Krickov, I. V., Pokrovsky, O. S., Manasypov, R. M., Lim, A., Shirokova, L. S., and Loiko, S.
841 V.: Colloidal transport of carbon and metals by western Siberian rivers during different
842 seasons across a permafrost gradient, *Geochim. Cosmochim. Acta* 265, 221-241,
843 <https://doi.org/10.1016/j.gca.2019.08.041>, 2019.

844 Kuzmina, D., Lim, A. G., Loiko, S. V., Shirokova, L. S., Julien, F., Rols, J. L., and Pokrovsky,
845 O. S.: Dispersed ice of permafrost peatlands represents an important source of labile
846 carboxylic acids, nutrients and metals, *Geoderma*, 429, Art No 116256.
847 <https://doi.org/10.1016/j.geoderma.2022.116256>, 2023.

848 Lapierre, J.-F., Guillemette, F., Berggren, M., and del Giorgio, P. A.: Increases in terrestrially
849 derived carbon stimulate organic carbon processing and CO₂ emissions in boreal aquatic
850 ecosystems, *Nature Comm.*, 4, 2972, doi:10.1038/ncomms3972, 2013.

851 Larouche, J. R., Abbott, B. W., Bowden, W. B., Jones, and J. B.: The role of watershed
852 characteristics, permafrost thaw, and wildfire on dissolved organic carbon biodegradability
853 and water chemistry in Arctic headwater streams, *Biogeosciences*, 12, 4221-4233,
854 <https://doi.org/10.5194/bg-12-4221-2015>, 2015.

855 Lau, M. P.: Linking the dissolved and particulate domain of organic carbon in inland waters. *J.*
856 *Geophys. Res.: Biogeosciences*, 126, e2021JG006266.
857 <https://doi.org/10.1029/2021JG006266>, 2021.

858 Laurion, I., and Mladenov, N.: Dissolved organic matter photolysis in Canadian Arctic thaw
859 ponds, *Environ. Res. Lett.*, 8, 035026, doi.org/10.1088/1748-9326/8/3/035026, 2013.

860 Laurion, I., Massicotte, P., Mazoyer, F., Negandhi, K., and Mladenov, N.: Weak mineralization
861 despite strong processing of dissolved organic matter in Eastern Arctic tundra ponds,
862 *Limnol. Oceanogr.*, 66, S47–S63, <https://doi.org/10.1002/lno.11634>, 2021.

863 Liu, F., and Wang, D.: Dissolved organic carbon concentration and biodegradability across the
864 global rivers: A meta-analysis, *Sci. Total Environ.*, 818, Art No 151828,
865 <https://doi.org/10.1016/j.scitotenv.2021.151828>, 2022.

866 Lou, T., and Xie, H.: Photochemical alteration of the molecular weight of dissolved organic
867 matter, *Chemosphere*, 65, 2333-2342, <https://doi.org/10.1016/j.chemosphere.2006.05.001>,
868 2006.

869 Mann, P. J., Davydova, A., Zimov, N., Spencer, R. G. M., Davydov, S., Bulygina, E., Zimov, S.,
870 Holmes, R. M.: Controls on the composition and lability of dissolved organic matter in
871 Siberia's Kolyma River basin, *J. Geophys. Res.*, 117, G01028, doi: 10.1029/2011JG001798,
872 2012.

873 Mann, P. J., Sobczak, W. V., LaRue, M. M., Bulygina, E., Davydova, A., Vonk, J. E., Schade,
874 J., Davydov, S., Zimov, N., Holmes, R. M., Spencer, R. G. M.: Evidence for key enzymatic
875 controls on metabolism of Arctic river organic matter, *Global Change Biol.*, 20(4), 1089-
876 1100, <https://doi.org/10.1111/gcb.12416>, 2014.

877 Mann, P. J., Eglinton, T. I., McIntyre, C. P., Zimov, N., Davydova, A., Vonk, J. E., Holmes, R.
878 M., Spencer, R. G. M.: Utilization of ancient permafrost carbon in headwaters of Arctic
879 fluvial networks, *Nat. Commun.*, 6, doi: 10.1038/ncomms8856, 2015.

880 Mazoyer, F., Laurion, I., and Rautio, M.: The dominant role of sunlight in degrading winter
881 dissolved organic matter from a thermokarst lake in a subarctic peatland, *Biogeosciences*,
882 19, 3959–3977, <https://doi.org/10.5194/bg-19-3959-2022>, 2022.

883 Moody, C. S., Worrall, F., Evans, C. D., Jones, T. G.: The rate of loss of dissolved organic carbon
884 (DOC) through a catchment, *J. Hydrol.*, 492, 139-150,
885 <https://doi.org/10.1016/j.jhydrol.2013.03.016>, 2013.

886 Moran, M. A., Sheldon, W. M., and Zepp, R. G.: Carbon loss and optical property changes during
887 long-term photochemical and biological degradation of estuarine dissolved organic matter,
888 *Limnol. Oceanogr.*, 45, 1254–1264, <https://doi.org/10.4319/lo.2000.45.6.1254>, 2000.

889 Mostofa, K. M. G., Yoshioka, T., Konohira, E., and Tanoue, E.: Photodegradation of fluorescent
890 dissolved organic matter in river waters, *Geochem. J.*, 41, 323-331,
891 <https://doi.org/10.2343/geochemj.41.323>, 2007.

892 Obernosterer, I., and Benner, R.: Competition between biological and photochemical processes
893 in the mineralization of dissolved organic carbon, *Limnol. Oceanogr.*, 49, 117–124,
894 <https://doi.org/10.4319/lo.2004.49.1.0117>, 2004.

895 Oleinikova, O., Drozdova, O. Y., Lapitskiy, S. A., Bychkov, A. Y., and Pokrovsky, O. S.:
896 Dissolved organic matter degradation by sunlight coagulates organo-mineral colloids and
897 produces low-molecular weight fraction of metals in boreal humic waters, *Geochim.*
898 *Cosmochim. Acta*, 211, 97-114, doi:10.1016/j.gca.2017.05.023, 2017.

899 Oleinikova, O., Shirokova, L. S., Drozdova, O. Y., Lapitsky, S. A., and Pokrovsky, O. S.: Low
900 biodegradability of dissolved organic matter and trace metal from subarctic waters by culturable
901 heterotrophic bacteria, *Sci. Total Environ.*, 618, 174-187,
902 <https://doi.org/10.1016/j.scitotenv.2017.10.340>, 2018.

903 Payandi-Rolland, D.; Shirokova, L.S.; Tesfa, M.; Lim, A.G.; Kuzmina, D.; Benezeth, P.;
904 Karlsson, J.; Giesler, R.; Pokrovsky, O.S.: Dissolved organic matter biodegradation along a
905 hydrological continuum in a discontinuous permafrost area: Case study of northern Siberia
906 and Sweden, *Sci. Total Environ.*, 749, Art No 141463,
907 <https://doi.org/10.1016/j.scitotenv.2020.141463>, 2020.

908 Peacock, M., Evans, C. D., Fenner, N., Freeman, C., Gough, R., Jones, T. G., and Lebron, I.:
909 UV-visible absorbance spectroscopy as a proxy for peatland dissolved organic carbon
910 (DOC) quantity and quality: considerations on wavelength and absorbance degradation,
911 *Environmental Science: Processes and Impacts*, 10–12, doi:10.1039/c4em00108g, 2014.

912 Pickard, A. E., Heal, K. V., McLeod, A. R., and Dinsmore, K. J.: Temporal changes in
913 photoreactivity of dissolved organic carbon and implications for aquatic carbon fluxes from
914 peatlands, *Biogeosciences*, 14, 1793–1809, <https://doi.org/10.5194/bg-14-1793-2017>, 2017.

915 Pokrovsky, O. S., Dupré, B., and Schott, J.: Fe-Al-organic colloids control the speciation of trace
916 elements in peat soil solutions: results of ultrafiltration and dialysis, *Aquatic Geochem.*, 11,
917 241–278, <http://dx.doi.org/10.1007/s10498-004-4765-2>, 2005.

918 Pokrovsky, O. S., Viers, J., Shirokova, L. S., Shevchenko, V. P., Filipov, A. S., and Dupré, B.:
919 Dissolved, suspended, and colloidal fluxes of organic carbon, major and trace elements in
920 Severnaya Dvina River and its tributary, *Chem. Geol.*, 273, 136–149,
921 <https://doi.org/10.1016/j.chemgeo.2010.02.018>, 2010.

922 Pokrovsky, O. S., Shirokova, L. S., Zabelina, S. A., Vorobieva, T. Ya., Moreva, O. Yu., Klimov,
923 S. I., Chupakov, A. V., Shorina, N. V., Kokryatskaya, N. M., Audry, S., Viers, J., Zoutien,
924 C., and Freydier, R.: Size fractionation of trace elements in a seasonally stratified boreal
925 lakes: Control of organic matter and iron colloids, *Aquat. Geochem.*, 18, 115–139,
926 <https://doi.org/10.5194/bg-16-2511-2019>, 2012.

927 Pokrovsky, O. S., Manasypov, R. M., Loiko, S. V., and Shirokova, L. S.: Organic and organo-
928 mineral colloids of discontinuous permafrost zone, *Geochim. Cosmochim. Ac.*, 188, 1–20,
929 <http://dx.doi.org/10.1016/j.gca.2016.05.035>, 2016.

930 Porcal, P., Dillon, P. J., and Molot, L. A.: Photochemical production and decomposition of
931 particulate organic carbon in a freshwater stream, *Aquat. Sci.*, 75, 469–482,
932 <http://dx.doi.org/10.1007/s00027-013-0293-8>, 2013.

933 Porcal, P., Dillon, P. J., and Molot, L. A.: Interaction of extrinsic chemical factors affecting
934 photodegradation of dissolved organic matter in aquatic ecosystems, *Photochem. Photobiol.*
935 *Sci.*, 13, 799–812, <http://dx.doi.org/10.1039/c4pp00011k>, 2014.

936 Porcal, P., Dillon, P. J., and Molot, L. A.: Temperature dependence of photodegradation of
937 dissolved organic matter to dissolved inorganic carbon and particulate organic carbon, *Plos*
938 *ONE*, 10(6), e0128884, doi:10.1371/journal.pone.0128884, 2015.

939 Prijac, A., Gandois, L., Jeanneau, L., Taillardat, P., and Garneau, M.: Dissolved organic matter
940 concentration and composition discontinuity at the peat–pool interface in a boreal peatland,
941 *Biogeosciences*, 19, 4571–4588, <https://doi.org/10.5194/bg-19-4571-2022>, 2022.

942 Raudina, T. V., Loiko, S. V., Lim, A., Manasypov, R. M., Shirokova, L. S., Istigecegev, G. I.,
943 Kuzmina, D. M., Kulizhsky, S. P., Vorobyev, S. N., and Pokrovsky, O. S.: Permafrost thaw
944 and climate warming may decrease the CO₂, carbon, and metal concentration in peat soil
945 waters of the Western Siberia Lowland, *Sci. Total Environ.*, 634, 1004–1023,
946 <http://dx.doi.org/10.1016/j.scitotenv.2018.04.059>, 2018.

947 Raudina, T. V., Loiko, S., Kuzmina, D. M., Shirokova, L. S., Kulizhsky, S. P., Golovatskaya, E.
948 A., and Pokrovsky, O. S.: Colloidal organic carbon and trace elements in peat porewaters
949 across a permafrost gradient in Western Siberia, *Geoderma* 390, Art No 114971,
950 <https://doi.org/10.1016/j.geoderma.2021.114971>, 2021.

951 Raudina, T. V., Smirnov, S. V., Luschaeva, I. V., Kulizhskiy, S. P., Golovatskaya, E. A.,
952 Shirokova, L.S., and Pokrovsky, O. S.: Seasonal and spatial variations of dissolved organic

953 matter biodegradation along the aquatic continuum in the southern taiga bog complex,
 954 Western Siberia. *Water (MDPI)*, 14, Art No 3969. <https://doi.org/10.3390/w1423396>, 2022.

955 Roehm, C. L., Giesler, R., Karlsson, J.: Bioavailability of terrestrial organic carbon to lake
 956 bacteria: The case of a degrading subarctic permafrost mire complex, *J. Geophys. Res.*, 114,
 957 G03006, doi: 10.1029/2008JG000863, 2009.

958 Rosset, T., Binet, S., Rigal, F., and Gandois, L.: Peatland dissolved organic carbon export to
 959 surface waters: Global significance and effects of anthropogenic disturbance, *Geophysical*
 960 *Res. Lett.*, 49, e2021GL096616. <https://doi.org/10.1029/2021GL096616>, 2022.

961 Selvam, B. P., Lapierre, J.-F., Guillemette, F., Voigt, C., Lamprecht, R. E., Biasi, C., Christensen,
 962 T. R., Martikainen P. J., and Berggren, M.: Degradation potentials of dissolved organic
 963 carbon (DOC) from thawed permafrost peat, *Scientific Reports*, 7, Art No 45811, doi:
 964 10.1038/srep45811, 2016.

965 Serikova, S., Pokrovsky, O. S., Ala-aho, P., Kazantsev, V., Kirpotin, S. N. Kopysov, S. G.,
 966 Krickov, I. V., Laudon, H., Manasypov, R. M., Shirokova, L. S., Sousby, C., Tetzlaff, D.,
 967 and Karlsson, J.: High riverine CO₂ emissions at the permafrost boundary of Western
 968 Siberia. *Nature Geoscience*, 11, 825-829, <https://www.nature.com/articles/s41561-018-0218-1>, 2018.

970 Serikova, S., Pokrovsky, O. S., Laudon, H., Krickov, I. V., Lim, A. G., Manasypov, R. M., and
 971 Karlsson, J.: C emissions from lakes across permafrost gradient of Western Siberia, *Nature*
 972 *Comm.* 10, Art No 1552, <https://doi.org/10.1038/s41467-019-09592-1>, 2019.

973 Shirokova, L. S., Bredoire, R., Rolls, J. L., and Pokrovsky, O. S.: Moss and peat leachate
 974 degradability by heterotrophic bacteria: fate of organic carbon and trace metals,
 975 *Geomicrobiol. J.*, 34(8), 641-655, <http://dx.doi.org/10.1080/01490451.2015.1111470>,
 976 2017a.

977 Shirokova, L. S., Chupakova, A. A., Chupakov, A. V., and Pokrovsky, O.S.: Transformation of
 978 dissolved organic matter and related trace elements in the mouth zone of the largest
 979 European Arctic river: experimental modeling, *Inland Waters*, 7(3), 272-282,
 980 <https://doi.org/10.6084/m9.figshare.5387686>, 2017b.

981 Shirokova, L. S., Labouret, J., Gurge, M., Gerard, E., Zabelina, S. A., Ivanova, I. S., Pokrovsky,
 982 O. S.: Impact of cyanobacterial associate and heterotrophic bacteria on dissolved organic
 983 carbon and metal in moss and peat leachate: application to permafrost thaw in aquatic
 984 environments, *Aquatic Geochemistry*, 23(5-6), 331-358, <https://doi.org/10.1007/s10498-017-9325-7>, 2017c.

986 Shirokova, L. S., Chupakov, A. V., Zabelina, S. A., Neverova, N. V., Payandi-Rolland, D.,
 987 Causseraund, C., Karlsson, J., and Pokrovsky, O. S.: Humic surface waters of frozen peat
 988 bogs (permafrost zone) are highly resistant to bio- and photodegradation, *Biogeosciences*,
 989 16, 2511-2526, <https://doi.org/10.5194/bg-16-2511-2019>, 2019.

990 Shirokova, L. S., Chupakov, A. V., Ivanova, I. S., Moreva, O. Y., Zabelina, S. A., Shutskiy, N.
 991 A., Loiko S. V., Pokrovsky, O. S. Lichen, moss and peat control of C, nutrient and trace
 992 metal regime in lakes of permafrost peatlands. *Science Total Environ.*, 782, Art No 146737,
 993 <https://doi.org/10.1016/j.scitotenv.2021.146737>, 2021.

994 Spencer, R. G. M., Mann, P. J., Dittmar, T., Eglinton, T. I., McIntyre, C., Holmes, R. M., Zimov,
 995 N., Stubbins, A.: Detecting the signature of permafrost thaw in Arctic rivers, *Geophys. Res.*
 996 *Lett.*, 42, 2830-2835, <https://doi.org/10.1002/2015GL063498>, 2015.

997 Stubbins, A., Spencer, R.G., Chen, H., Hatcher, P.G., Mopper, K.W., Hernes, P.J., Mwamba,
 998 V., Mangangu, A.M., Wabakanhanzi, J.N., and Six, J.: Illuminated darkness: Molecular
 999 signatures of Congo River dissolved organic matter and its photochemical alteration as

1000 revealed by ultrahigh precision mass spectrometry. *Limnol. Oceanogr.*, 55(4), 1467-1477,
1001 10.4319/lo.2010.55.4.1467, 2010.

1002 Stutter, M. I., Richards, S., and Dawson, J. J. C.: Biodegradability of natural dissolved organic
1003 matter collected from a UK moorland stream, *Water Res.*, 47(3), 1169-1180,
1004 <https://doi.org/10.1016/j.watres.2012.11.035>, 2013.

1005 Sulzberger, B., Austin, A. T., Cory, R. M., Zepp, R. G., and Paul, N. D.: Solar UV radiation in
1006 a changing world: roles of cryosphere-land-water-atmosphere interfaces in global
1007 biogeochemical cycles, *Photochem. Photobiol. Sci.*, doi: 10.1039/c8pp90063a, 2019.

1008 Taillardat, P., Bodmer, P., Deblois, C. P., Ponçot, A., Prijac, A., Riahi, K., et al. : Carbon
1009 dioxide and methane dynamics in a peatland headwater stream: Origins, processes and
1010 implications, *J. Geophysical Res.: Biogeosciences*, 127, e2022JG006855.
1011 <https://doi.org/10.1029/2022JG006855>, 2022.

1012 Textor, S. R., Guillemette, F., Zito, P. A., Spencer, R. G. M.: An assessment of dissolved
1013 organic carbon biodegradability and priming in blackwater systems, *J. Geophys. Res.*
1014 *Biogeosciences*, 123(9), 2998-3015, <https://doi.org/10.1029/2018JG004470>, 2018.

1015 Tranvik, L. J., Downing, J. A., Cotner, J. B., Loiselle, S. A., Striegl, R. G., Ballatore, T. J.,
1016 Dillon, P., Finlay, K., Fortino, K., Knoll, L. B., Kortelainen, P. L., Kutser, T., Larsen, S.,
1017 Laurion, I., Leech, D. M., McCallister, S. L., McKnight, D. M., Melack, J. M., Overholt,
1018 E., Porter, J. A., Prairie, Y., Renwick, W. H., Roland, F., Sherman, B. S., Schindler, D. W.,
1019 Sobek, S., Tremblay, A., Vanni, M. J., Verschoor, A. M., von Wachenfeldt, E., and
1020 Weyhenmeyer, G. A.: Lakes and reservoirs as regulators of carbon cycling and climate,
1021 *Limnol. Oceanogr.*, 54, 2298–2314, https://doi.org/10.4319/lo.2009.54.6_part_2.2298,
1022 2009.

1023 Vachon, D., Lapiere, J., and del Giorgio, P. A.: Seasonality of photochemical dissolved
1024 organic carbon mineralization and its relative contribution to pelagic CO₂ production in
1025 northern lakes, *J. Geophys. Res.-Biogeo.*, 121, 864–878,
1026 <https://doi.org/10.1002/2015JG003244>, 2016.

1027 Vachon, D., Solomon, C. T., and del Giorgio, P. A.: Reconstructing the seasonal dynamics and
1028 relative contribution of the major processes sustaining CO₂ emissions in northern lakes,
1029 *Limnol. Oceanogr.*, 62, 706–722, <https://doi.org/10.1002/lno.10454>, 2017.

1030 Vähätalo, A. V., Salonen, K., Münster, U., Järvinen, M., and Wetzel, R. G.: Photochemical
1031 transformation of allochthonous organic matter provides bioavailable nutrients in a humic
1032 lake, *Acta Hydrobiol.*, 156, 287-314, <http://dx.doi.org/10.1127/0003-9136/2003/0156-0287>,
1033 2003.

1034 Vähätalo, A. V. and Wetzel, R.G.: Photochemical and microbial decomposition of chromophoric
1035 dissolved organic matter during long (months-years) exposures, *Mar. Chem.*, 89, 313-326,
1036 <http://dx.doi.org/10.1016/j.marchem.2004.03.010>, 2004.

1037 Vasyukova, E., Pokrovsky, O. S., Viers, J., Oliva, P., Dupré, B., Martin, F., and Candaudap, F.:
1038 Trace elements in organic- and iron-rich surficial fluids of boreal zone: Assessing colloidal
1039 forms via dialysis and ultrafiltration, *Geochim. Cosmochim. Acta*, 74, 449-468,
1040 <https://doi.org/10.1016/j.crte.2012.08.003>, 2010.

1041 Vonk, J. E., Tank, S. E., Mann, P. J., Spencer, R. G. M., Treat, C. C., Striegl, R. G., Abbott,
1042 B. W., and Wickland K. P.: Biodegradability of dissolved organic carbon in permafrost
1043 soils and aquatic systems: a meta-analysis, *Biogeosciences*, 12, 6915-6930,
1044 <https://doi.org/10.5194/bg-12-6915-2015>, 2015.

1045 Ward, C. P., Nalven, S. G., Crump, B. C., Kling, G. W., and Cory, R. M.: Photochemical
1046 alteration of organic carbon draining permafrost soils shifts microbial metabolic pathways
1047 and stimulates respiration, *Nature Comm.*, 8, Art No 772,
1048 <https://www.nature.com/articles/s41467-017-00759-2>, 2017.

1049 Wauthy, M., Rautio, M., Christoffersen, K. S., Forsstrom, L., Laurion, I., Mariash, H. L.,
1050 Peura, S., Vincent, W. F.: Increasing dominance of terrigenous organic matter in
1051 circumpolar freshwaters due to permafrost thaw, *Limnol. Oceanogr. Lett.*, 3, 2018, 186–
1052 198, <http://dx.doi.org/10.1002/lo12.10063>, 2012.

1053 Weishaar, J. L., Aiken, G. R., Bergamaschi, B. A., Fram, M. S., Fujii, R., and Mopper, K.:
1054 Evaluation of specific ultraviolet absorbance as an indicator of the chemical composition
1055 and reactivity of dissolved organic carbon, *Environ. Sci. Technol.*, 37, 4702–4708,
1056 <http://dx.doi.org/10.1021/es030360x>, 2003.

1057 Wickland, K. P., Aiken G. R., Butler K., Dornblaser M. M., Spencer R. G. M., and Striegl R.
1058 G.: Biodegradability of dissolved organic carbon in the Yukon River and its tributaries:
1059 seasonality and importance of inorganic nitrogen. *Glob Biogeochem Cycle* 26,
1060 2012gb004342, <http://dx.doi.org/10.1029/2012GB004342>, 2012.

1061 Wilske, C., Herzsprung, P., Lechtenfeld, O.J., Kamjunke, N., and von Tümpling, W.:
1062 Photochemically induced changes of dissolved organic matter in a humic-rich and forested
1063 stream, *Water*, 12, 331. <https://doi.org/10.3390/w12020331>, 2020.

1064 Winter, A. R., Fish, T. A. E., Playle, R. C., Smith, D. S., and Curtis, P. J.: Photodegradation of
1065 natural organic matter from diverse freshwater sources, *Aquat. Toxicol.*, 84, 215-222,
1066 <https://doi.org/10.1016/j.aquatox.2007.04.014>, 2007.

1067 Zabelina, S.A., Shirokova, L.S., Klimov, S.I., Chupakov, A.V., Lim, A.G., Polishchuk, Y.M.,
1068 Polishchuk, V.Y., Bogdanov, A.N., Muratov, I.N., Guerin, F., Karlsson, J., and Pokrovsky,
1069 O.S.: Carbon emission from thermokarst lakes in NE European tundra, *Limnol. Oceanogr.*,
1070 66, S216-S230. <https://doi.org/10.1002/lno.11560>, 2021.

1071

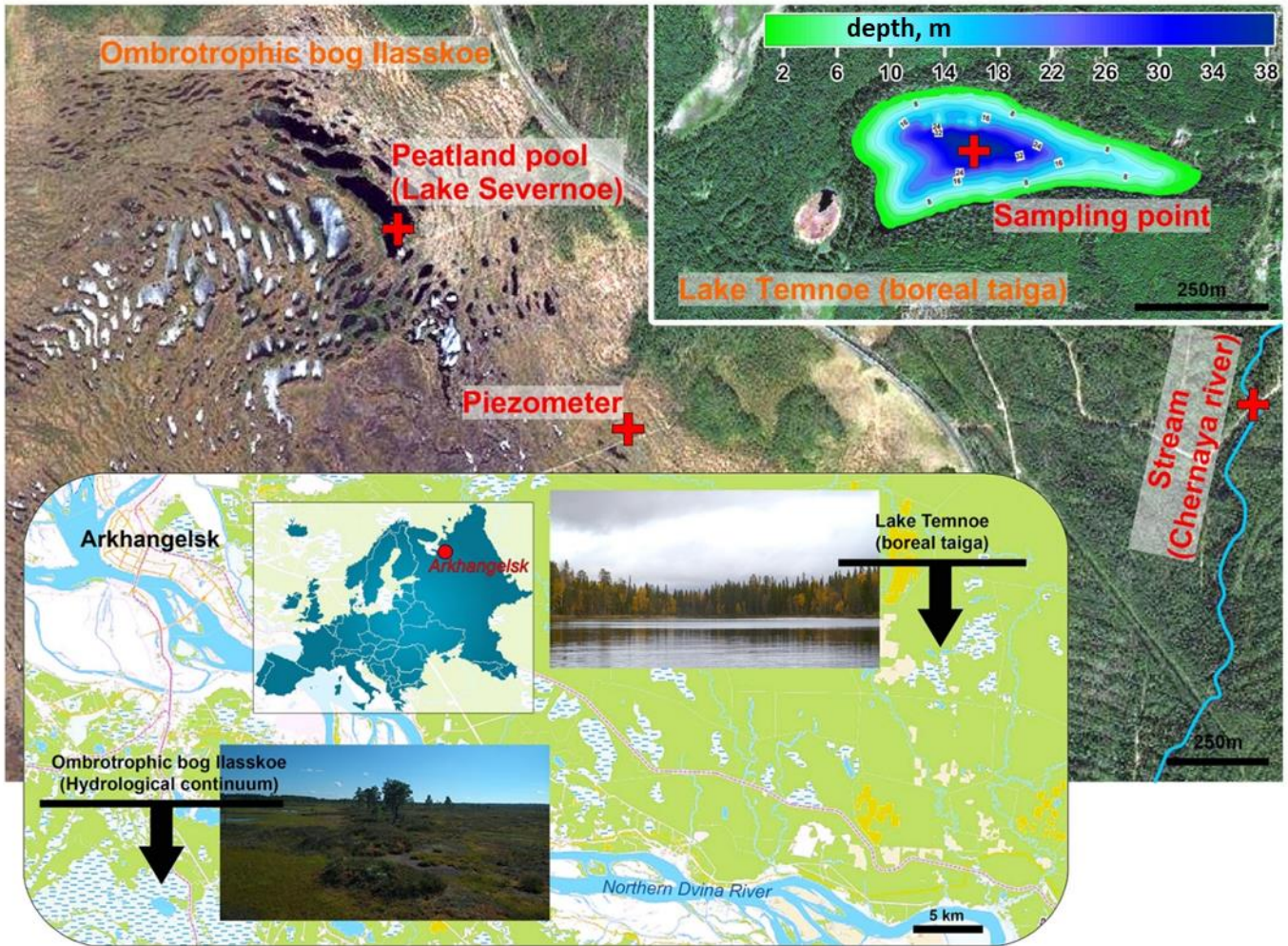
1072

1073

1074

1075

1076



1077

1078

1079

Fig. 1. Geographical location of studied hydrological continuum for Ilasskoe Bog waters and deep stratified Lake Temnoe in the boreal forest. Photo and map credits of Chupakov A.V.

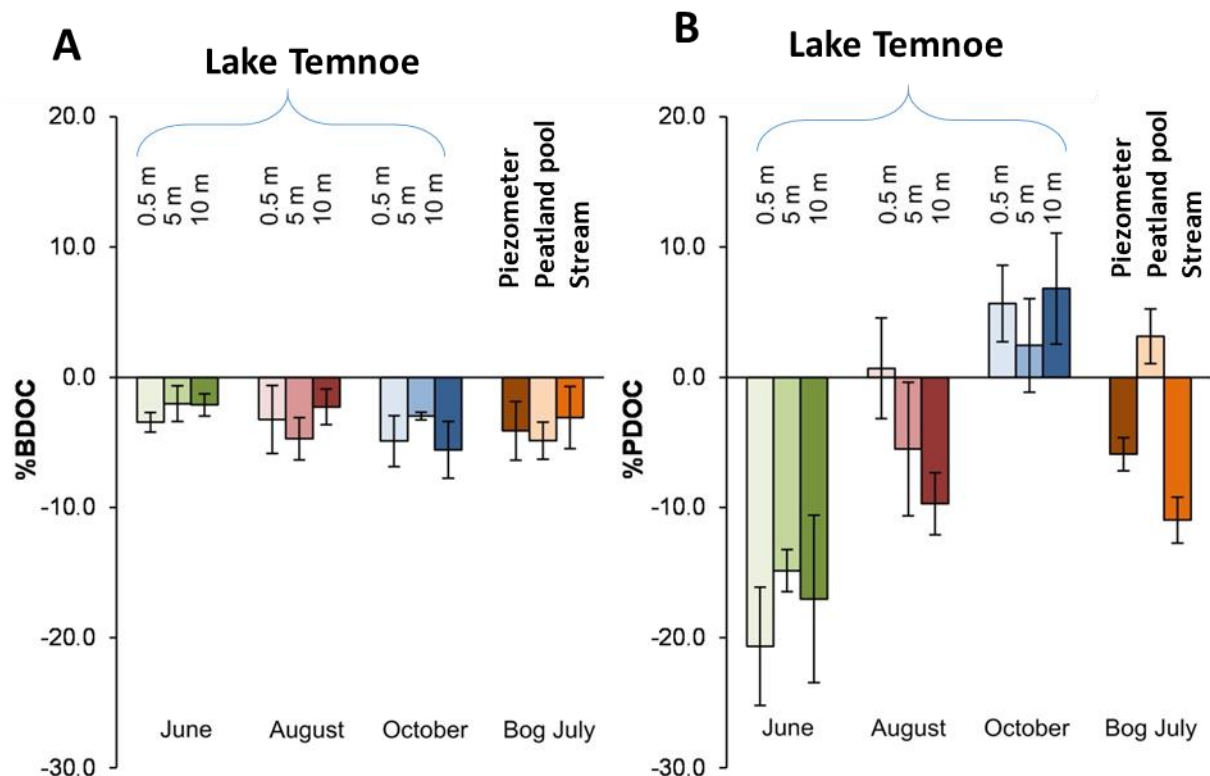
1081

1082

1083

1084

1085



1086

1087

1088

1089

1090 **Fig. 2.** Percentage of bio- (A) and photo- (B) degradable DOC presented as relative decrease in
 1091 DOC concentration between the initial and final value for the Temnoe Lake (June, August and
 1092 October) and Ilasskoe Bog surface waters (July). Error bars are 1 s.d. of duplicates relative to
 1093 the control (see Eqn. 1-2 in the text). In accord with unified protocol of biodegradation
 1094 experiments (Vonk et al., 2015), positive values signify nil photodegradation (experimental
 1095 artifacts of DOC production).

1096

1097

1098

1099

1100

1101

1102

1103

1104

1105

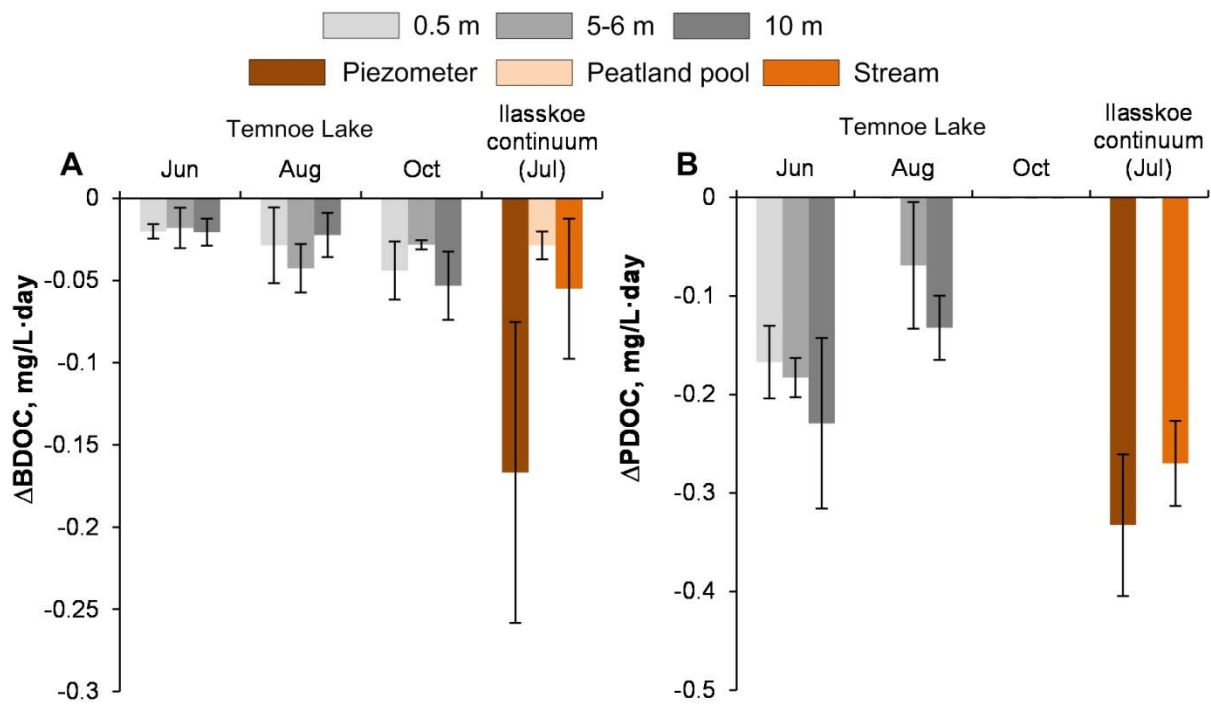
1106

1107

1108

1109

1110



1111

1112

1113

1114 **Fig. 3.** Rates of DOC bio- (A) and photo- (B) degradation. The values are negative because

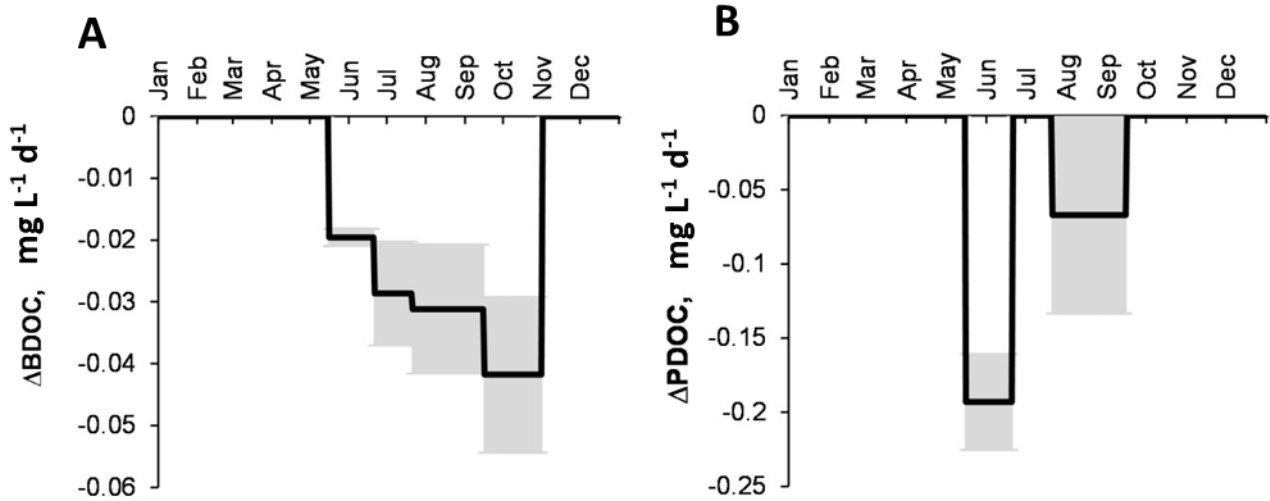
1115 they represent a decrease in DOC concentration over the course of the experiment.

1116

1117

1118

1119



1120

1121

1122

1123 **Fig. 4.** Integral rates of bio- (ΔBDOC , **A**) and photo- (ΔPDOC , **B**) degradation in the 0-10 m
 1124 layer of Lake Temnoe across the entire open-water period (May to October). Rate values are
 1125 negative because they signify a decrease in DOC concentration. Note that there was no
 1126 sampling from December to April and the photodegradation was not studied in July.
 1127 Uncertainties are represented by gray shaded rectangles.

1128

1129

1130

1131

1132

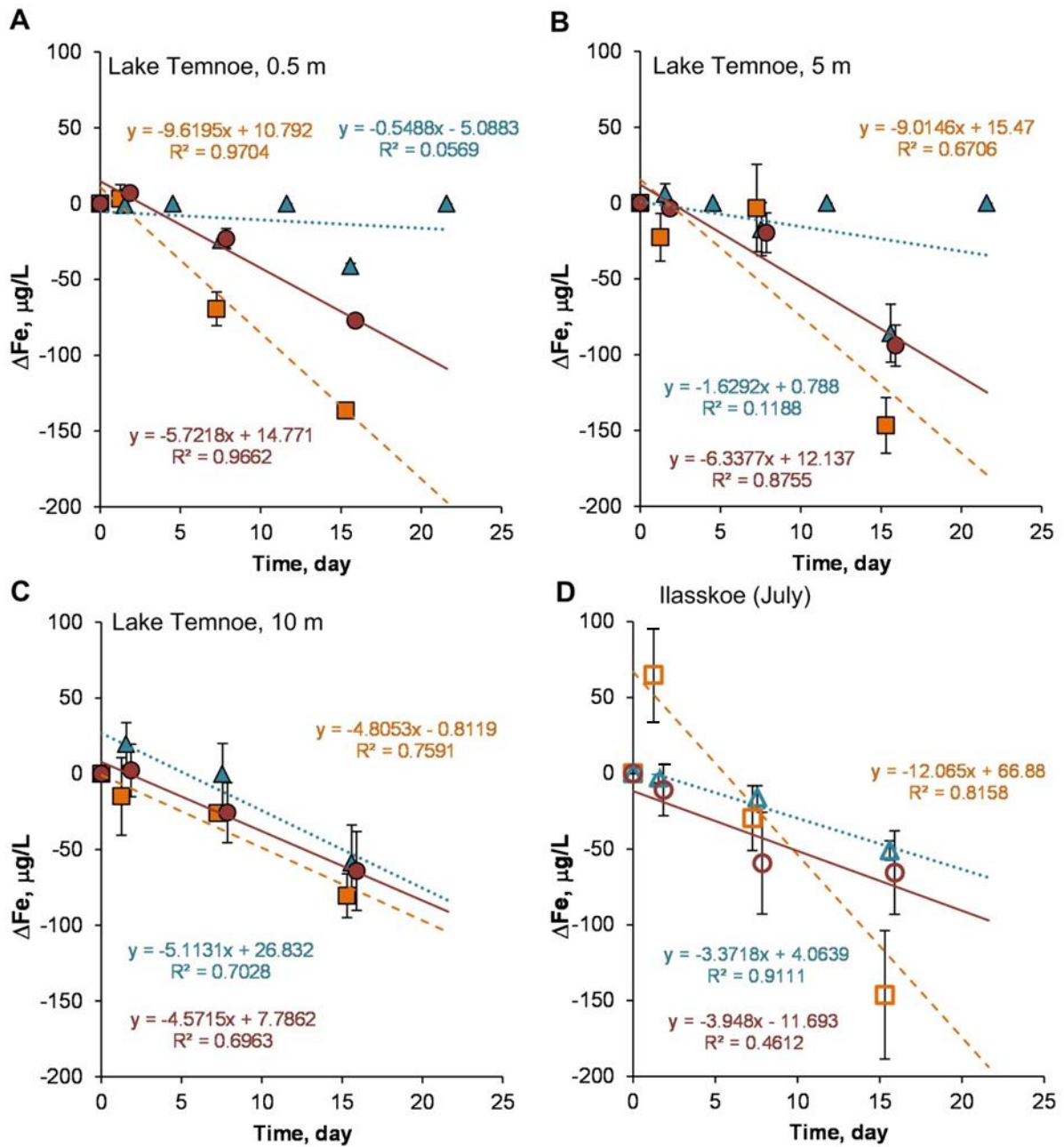
1133

1134

1135

1136

1137



1138

■ June ▲ August ● October □ Piezometer ▲ Peatland pool ○ Stream

1139

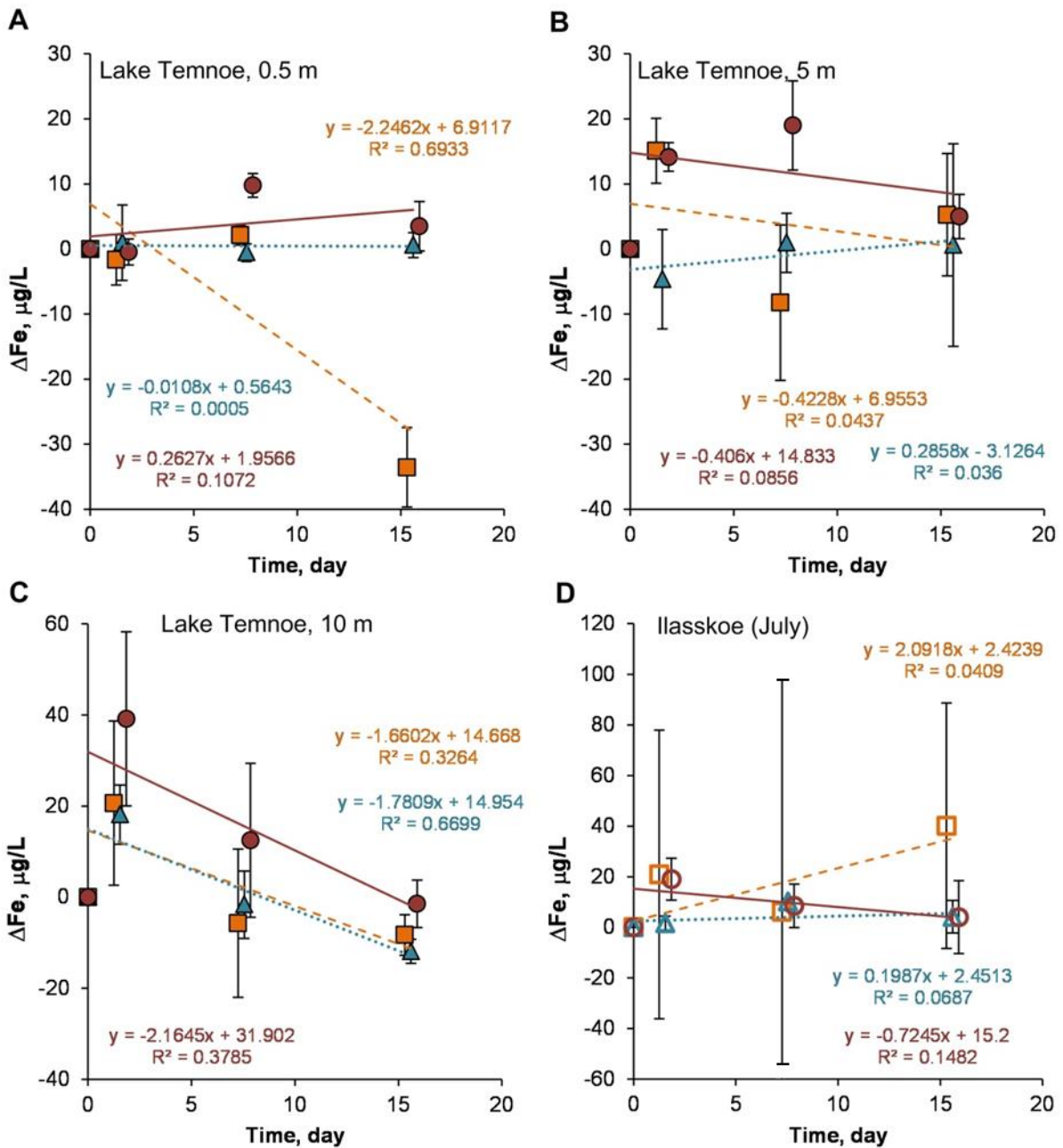
1140 **Fig. 5.** Change in Fe concentration (relative to control) over time in biodegradation
 1141 experiments. Error bars are 1 s.d. of duplicates. Temnoe Lake 0.5 m (A), 5 m (B) and 10 m (C)
 1142 in June (squares), August (triangles) and October (circles). Ilasskoe Bog continuum in July (D)
 1143 including piezometer (squares), Severnoe peatland pool (triangles) and stream Chernyi
 1144 (circles).

1145

1146

1147

1148



■ June
 ▲ August
 ● October
 Piezometer
 ▲ Peatland pool
 Stream

1149
 1150
 1151
 1152
 1153
 1154
 1155
 1156
 1157
 1158
 1159

Fig. 6. Change in Fe concentration (relative to the control) over time in photo-degradation experiments. The error bars are 1 s.d. of duplicates. Lake Temnoe 0.5 m (A), 5 m (B) and 10 m (C) in June (squares), August (triangles) and October (circles). Ilasskoe continuum in July (D) includes piezometer (squares), peatland pool Severnoe (triangles) and stream Chernyi (circles)

1160 **Table 1.** Landscape setting, hydrochemical characteristics and CO₂ concentration and emission
 1161 flux of studied waters. S.C. is specific conductivity and EB and OB is eutrophic and
 1162 oligotrophic bacteria count, respectively.

1163 **1A.** Plasskoe bog continuum in July.

1164

	Piezometer	Lake Severnoe	Stream Chernyi
GPS coordinates	N64.328694° E40.612556°	N64.334361° E40.609667°	N64.330982° E40.653352°
Description	Shallow groundwater	Peatland pool	Outlet stream
T, °C	11.4	19.4	13
O₂, mg/L	0.6	8.6	7.5
pH	3.9	4.0	5.7
S.C., μS cm⁻¹	46	17	26
DOC, mg L⁻¹	87.6	12.7	38.4
DIC, mg L⁻¹	0.32	0.40	0.38
SUVA₂₅₄	4.13	3.80	4.85
P-PO₄, μg L⁻¹	8.6	3.0	1.7
P_{total}, μg L⁻¹	153	10	20
N-NO₃, μg L⁻¹	111	70	98
N-NH₄, μg L⁻¹	85.4	16.1	12.6
N_{total}, μg L⁻¹	1180	222	399
Si, μg L⁻¹	1808	47	2076
CO₂, μmol/L	3360	55	318
CO₂ flux, mmol m⁻² d⁻¹	1600	22	151
EB, CFU mL⁻¹	49360	56600	9000
OB, CFU mL⁻¹	54560	37900	21600

1165

1166 **1B.** Lake Temnoe across seasons and depths.

1167

1168

Month	Jun	Jun	Jun	Aug	Aug	Aug	Oct	Oct	Oct
	0.5	5	10	0.5	5	10	0.5	6	10
GPS	N64.47683° E041.74533°								
Description	Lake in the northern taiga								
T, °C	12.7	4,9	4,5	18.4	5.5	4.3	9.0	5.8	4.4
O₂, mg/L	8,45	4,8	4,5	7.78	4.93	2.63	8.90	4.46	2.14
pH	5.2	5.2	5.3	6.0	5.5	5.7	5.2	5.2	5.1
S.C., μS cm⁻¹	17	17	19	17	17	19	18	18	20
DOC, mg L⁻¹	12.6	19.2	21	19	19.5	21.2	19.4	20.6	20.6
DIC, mg L⁻¹	0.55	0.53	0.49	0.70	0.71	0.66	0.67	0.67	0.64
SUVA₂₅₄	4.6	4.7	4.6	4.2	4.5	4.5	4.3	4.3	4.7
P-PO₄, μg L⁻¹	2.9	3.3	6.4	0.9	3.6	9.4	3.8	4.6	4.2
P_{total}, μg L⁻¹	19	17	19	20	16	20	18	19	20
N-NO₃, μg L⁻¹	119	150	137	86	152	254	88	85	100
N-NH₄, μg L⁻¹	7.1	8.0	10.0	9.1	17.5	13.8	16.4	14.1	15.5
N_{total}, μg L⁻¹	305	420	408	355	315	337	425	416	396
Si, μg L⁻¹	1940	2268	2354	1183	2208	2714	2269	2380	2380
CO₂, μmol/L	99	309	329	110	256	337	223	232	253
CO₂ flux, mmol m⁻² d⁻¹	32	-	-	46	-	-	71	-	-
EB, CFU mL⁻¹	-	36	50	259	92	270	780	220	105
OB, CFU mL⁻¹	50	570	420	-	190	-	680	150	66

1169

Table 2. The % bio- and photodegradable solutes (mean \pm s.d.) whose relative change (concentration decrease) in the course of experiment was superior to that of SD. Prefix ΔB and ΔP represents the effect of bio- and photodegradation, respectively. Duration of biodegradation and photodegradation is 21.6 ± 0.1 and 15.6 ± 0.1 days, respectively. W represents the probability of measurable effect, significantly different from changes in the control reactors. Only the components with $W \geq 33\%$ are presented. Temnoe Lake is deep stratified lake in the forest. Peizometer, peatland pool and outlet stream represent the hydrological continuum of the Illasskoe Bog.

Index	Temnoe Lake		Temnoe Lake		Temnoe Lake		Temnoe Lake		Temnoe Lake		Temnoe Lake		Piezo-meter (Jul)		Peatland pool (Jul)		Outlet stream (Jul)	
	0.5 m (Jun)	5 m (Jun)	10 m (Jun)	0.5 m (Aug)	5 m (Aug)	10 m (Aug)	0.5 m (Oct)	5 m (Oct)	10 m (Oct)	0.5 m (Oct)	6 m (Oct)	10 m (Oct)	10 m (Oct)					
$\bar{\alpha}$, $\mu S/cm$	17	17	19	17	17	19	18	18	19	18	18	20	20	46	17	26		
$\Delta B(\bar{\alpha} \pm SD)$	-24 \pm 4	-26 \pm 7	-30 \pm 5	-23 \pm 3	-27 \pm 3	-33 \pm 16	-24 \pm 7	-23 \pm 4	-33 \pm 16	-24 \pm 7	-23 \pm 4	-17 \pm 5	-17 \pm 5	0	-18 \pm 10	-29 \pm 4		
DOC, mg/L	12.6	19.2	21.0	19.0	19.5	21.2	19.4	20.6	21.2	19.4	20.6	20.6	20.6	87.6	12.7	38.4		
$\Delta B(DOC \pm SD)$	3.4 \pm 0.8	2.0 \pm 1.4	2.1 \pm 0.8	3.2 \pm 2.6	4.7 \pm 1.6	2.3 \pm 1.4	4.9 \pm 2.0	3.0 \pm 0.3	2.3 \pm 1.4	4.9 \pm 2.0	3.0 \pm 0.3	5.6 \pm 2.2	5.6 \pm 2.2	4.1 \pm 2.3	4.9 \pm 1.4	3.1 \pm 2.4		
$\Delta P(DOC \pm SD)$	20.7 \pm 4.6	14.9 \pm 1.6	17.0 \pm 6.4	0	5.5 \pm 5.1	9.7 \pm 2.4	0	0	9.7 \pm 2.4	0	0	0	0	5.9 \pm 1.3	0	11.0 \pm 1.8		
Al, $\mu g/L$	275	298	329	254	296	335	275	288	335	275	288	323	323	276	59	388		
$\Delta B(Al \pm SD)$	3.5 \pm 1.4	1.8 \pm 0.9	0	2.0 \pm 1.3	0	1.4 \pm 1.5	2.0 \pm 1.9	0	1.4 \pm 1.5	2.0 \pm 1.9	0	0	0	0.9 \pm 2.2	0	1.3 \pm 1.8		
$\Delta P(Al \pm SD)$	1.9 \pm 1.1	2.7 \pm 0.9	3.6 \pm 1.3	0	2.5 \pm 1.3	1.7 \pm 2.0	0.7 \pm 0.9	0	1.7 \pm 2.0	0.7 \pm 0.9	0	0	0	0	0	0.8 \pm 0.9		
Ti, $\mu g/L$	1.5	2.1	2.6	1.1	2.0	2.6	1.7	1.9	2.6	1.7	1.9	2.5	2.5	3.7	0.6	5.0		
$\Delta B(Ti \pm SD)$	-9.2 \pm 1.6	-9.9 \pm 7.4	-2.6 \pm 2.7	-4.8 \pm 3.4	-1.8 \pm 2.7	0	-3.6 \pm 1.7	-1.0 \pm 3.1	0	-3.6 \pm 1.7	-1.0 \pm 3.1	-1.0 \pm 3.9	-1.0 \pm 3.9	-2.3 \pm 3.6	-2.2 \pm 1.7	-1.4 \pm 2.2		
$\Delta P(Ti \pm SD)$	-0.1 \pm 3	-3 \pm 3	-8 \pm 3	0 \pm 0	-9 \pm 1	-3 \pm 2	-2 \pm 4	0	-3 \pm 2	-2 \pm 4	0	0	0	0	-20 \pm 4	-3.3 \pm 0.5		
V, $\mu g/L$	0.5	0.6	0.7	0.4	0.5	0.7	0.4	0.5	0.7	0.4	0.5	0.7	0.7	1.1	0.5	1.3		
$\Delta B(V \pm SD)$	-8.3 \pm 16.2	-5.4 \pm 3.2	-4.9 \pm 2.3	-6.8 \pm 7.5	-10.0 \pm 4.6	-1.7 \pm 1.6	-14.7 \pm 11	-13.9 \pm 4.3	-1.7 \pm 1.6	-14.7 \pm 11	-13.9 \pm 4.3	-16.1 \pm 1.7	-16.1 \pm 1.7	-3.2 \pm 2.6	-0.2 \pm 3.4	-17.9 \pm 5.0		
Mn, $\mu g/L$	39	55	79	17	48	93	30	47	93	30	47	105	105	78	9	47		
$\Delta B(Mn \pm SD)$	0	0	-0.3 \pm 2.2	-31.8 \pm 1.3	-3.2 \pm 1.6	-0.6 \pm 2.2	-4.8 \pm 2.2	-3.2 \pm 1.7	-0.6 \pm 2.2	-4.8 \pm 2.2	-3.2 \pm 1.7	-0.4 \pm 0.1	-0.4 \pm 0.1	0	0	-1.6 \pm 2.8		
Fe, $\mu g/L$	358	527	710	165	460	795	317	448	795	317	448	820	820	4402	157	1006		
$\Delta B(Fe \pm SD)$	-18.1 \pm 2.5	-9.1 \pm 2.6	-5.4 \pm 1.6	-13.5 \pm 1.0	-6.3 \pm 2.6	-1.4 \pm 1.9	-9.5 \pm 1.4	-7.8 \pm 1.9	-1.4 \pm 1.9	-9.5 \pm 1.4	-7.8 \pm 1.9	-3.3 \pm 1.8	-3.3 \pm 1.8	-0.8 \pm 0.8	-13.6 \pm 4.3	-4.5 \pm 2.4		
$\Delta P(Fe \pm SD)$	-3.9 \pm 0.6	-2.0 \pm 1.9	-4.0 \pm 1.3	0	-2.9 \pm 1.5	-0.2 \pm 0.6	-1.2 \pm 0.4	0	-0.2 \pm 0.6	-1.2 \pm 0.4	0	0	0	0	0	0		

Index	Temnoe Lake 0.5 m (Jun)		Temnoe Lake 5 m (Jun)		Temnoe Lake 10 m (Jun)		Temnoe Lake 0.5 m (Aug)		Temnoe Lake 5 m (Aug)		Temnoe Lake 10 m (Aug)		Temnoe Lake 0.5 m (Oct)		Temnoe Lake 6 m (Oct)		Temnoe Lake 10 m (Oct)		Piezometer (Jul)	Peatland pool (Jul)	Outlet stream (Jul)	
Co, µg/L	0.28	0.39	0.68	0.07	0.30	0.65	0.18	0.31	0.74	0.45	0.06	0.30	0.45	0.06	0.30	0.45	0.06	0.30	0.45	0.06	0.30	0.30
ΔB(Co±SD)	-2.2±5.1	-1.2±2.1	-3.7±4.6	-32.7±2.6	-8.1±5.6	-2.7±3.3	-11.0±4.4	-9.1±5.1	-1.6±0.4	0	0	0	0	0	0	0	0	0	0	0	0	-20.6±27.8
Cu, µg/L	0.5	0.6	0.7	0.6	0.6	0.7	0.7	0.7	0.5	1.5	0.3	0.8	1.5	0.3	0.8	1.5	0.3	0.8	1.5	0.3	0.8	0.8
ΔB(Cu±SD)	0	0	0	-14.3±1.4	-6.8±4.0	-17.9±11.0	-5.3±4.8	-4.1±8.0	-1.4±12.3	0	0	0	0	0	0	0	0	0	0	0	0	-7.7±9.9
Ga, µg/L	0.017	0.022	0.026	0.012	0.016	0.023	0.017	0.015	0.024	0.126	0.016	0.066	0.126	0.016	0.066	0.126	0.016	0.066	0.126	0.016	0.066	0.066
ΔP(Ga±SD)	-14±6	-13±5	-10±4	0	-1±8	0	-10±4	0	0	-7±5	-5±8	-6±3	-7±5	-5±8	-6±3	-7±5	-5±8	-6±3	-7±5	-5±8	-6±3	-6±3
Y, µg/L	0.22	0.25	0.28	0.20	0.24	0.28	0.22	0.23	0.28	0.10	0.01	0.21	0.10	0.01	0.21	0.10	0.01	0.21	0.10	0.01	0.21	0.21
ΔP(Y±SD)	-1.3±4.6	-6.7±0.9	-5.3±2.5	0	-2.3±0.7	-1.0±1.6	-1.4±0.2	0	0	0	0	0	0	0	0	0	0	0	0	0	0	-5.8±2.7
Zr, µg/L	0.4	0.4	0.5	0.4	0.5	0.5	0.4	0.4	0.5	0.3	0.1	0.4	0.3	0.1	0.4	0.3	0.1	0.4	0.3	0.1	0.4	0.4
ΔP(Zr±SD)	-15±4	-14±0	-13±2	-9±20	-17±1	-14±3	-4±4	0	0	0	0	0	0	0	0	0	0	0	0	0	0	-32±3
Nb, µg/L	0.016	0.020	0.025	0.012	0.020	0.024	0.017	0.018	0.025	0.033	0.005	0.042	0.033	0.005	0.042	0.033	0.005	0.042	0.033	0.005	0.042	0.042
ΔB(Nb±SD)	-3.6±10.2	-1.7±7.0	0	-7.7±4.8	-1.1±2.6	0	-7.3±2.3	-1.5±6.3	-5.0±4.0	-2.4±1.5	0	0	-2.4±1.5	0	0	-2.4±1.5	0	0	-2.4±1.5	0	0	0
ΔP(Nb±SD)	-9±3	-8±3	-9±1	-6±23	-13±2	-10±5	-8±4	0	-3±3	0	0	0	0	0	0	0	0	0	0	0	0	-10±4
Ba, µg/L	4.8	5.1	5.8	4.6	5.0	5.7	4.9	4.8	5.6	54.4	1.5	56.8	54.4	1.5	56.8	54.4	1.5	56.8	54.4	1.5	56.8	56.8
ΔB(Ba±SD)	-2.2±0.7	-2.8±1.7	-1.0±2.7	0	0	0	-1.9±0.5	-1.7±3.7	-5.9±1.6	0	0	0	0	0	0	0	0	0	0	0	0	-1.3±3.4
La, µg/L	0.23	0.26	0.30	0.21	0.26	0.32	0.24	0.27	0.31	0.07	0.01	0.22	0.07	0.01	0.22	0.07	0.01	0.22	0.07	0.01	0.22	0.22
ΔB(La±SD)	-4.9±6.5	0	0	-3.9±0.9	-0.3±1.6	-2.6±1.5	-1.1±3.6	-2.4±1.2	-4.0±2.8	-0.8±10.4	-29.7±10.0	-2.0±2.8	-0.8±10.4	-29.7±10.0	-2.0±2.8	-0.8±10.4	-29.7±10.0	-2.0±2.8	-0.8±10.4	-29.7±10.0	-2.0±2.8	-2.0±2.8
ΔP(La±SD)	-3.8±3.6	-1.2±5.9	-2.0±2.7	0	-3.6±1.0	-3.2±1.6	-1.8±0.9	-2.6±1.0	0	0	0	0	0	0	0	0	0	0	0	0	0	0
Ce, µg/L	0.58	0.65	0.71	0.50	0.62	0.78	0.59	0.63	0.78	0.21	0.03	0.56	0.21	0.03	0.56	0.21	0.03	0.56	0.21	0.03	0.56	0.56
ΔB(Ce±SD)	-5.2±4.2	0	0	-4.4±0.7	-0.1±1.4	-0.8±1.0	-0.9±2.9	-0.8±1.1	-2.2±2.2	0	0	0	0	0	0	0	0	0	0	0	0	-2.0±1.9
ΔP(Ce±SD)	-4.9±1.9	-6.2±1.2	-1.1±1.7	0	-1.5±0.5	-3.2±1.7	-1.9±1.2	0	-0.047±0.46	-3.7±1.5	-2.4±1.6	-3.6±1.1	-3.7±1.5	-2.4±1.6	-3.6±1.1	-3.7±1.5	-2.4±1.6	-3.6±1.1	-3.7±1.5	-2.4±1.6	-3.6±1.1	-3.6±1.1

1172
1173
1174

Table 2, continued.

Index	Temnoe Lake 0.5 m (Jun)		Temnoe Lake 5 m (Jun)		Temnoe Lake 10 m (Jun)		Temnoe Lake 0.5 m (Aug)		Temnoe Lake 5 m (Aug)		Temnoe Lake 10 m (Aug)		Temnoe Lake 0.5 m (Oct)		Temnoe Lake 6 m (Oct)		Temnoe Lake 10 m (Oct)		Piezometer (Jul)	Peatland pool (Jul)	Outlet stream (Jul)		
	Mean	SD	Mean	SD	Mean	SD	Mean	SD	Mean	SD	Mean	SD	Mean	SD	Mean	SD	Mean	SD	Mean	SD	Mean	SD	
Pr, µg/L	0.075	0.085	0.094	0.069	0.082	0.082	0.105	0.077	0.084	0.102	0.027	0.005	0.070	0.027	0.005	0.070	0.027	0.005	0.070	0.027	0.005	0.070	
ΔB(Pr±SD)	-1.9±5.2	0	-4.0±1.1	0	-0.7±1.3	0	-0.9±1.6	0	-3.2±2.3	-3.0±3.9	-5.5±0.9	-0.4±2.9	13.7±20.8	-6.1±2.8	0	-1.3±1.8	0	-0.01±2.4	-16.9±3.0	-2.4±2.1	-3.0±1.7	-10.8±8.4	-1.7±2.3
ΔP(Pr±SD)	0.33	0.34	0.39	0.29	0.33	0.33	0.42	0.33	0.32	0.41	0.11	0.02	0.27	0.11	0.02	0.27	0.11	0.02	0.27	0.11	0.02	0.27	
Nd, µg/L	-7.8±2.4	-4.5±2.5	-0.8±2.1	0	-3.8±2.5	-2.0±3.3	0	-0.8±4.7	-3.0±4.0	-8.7±8.4	-6.9±4.2	-23.7±8.6	-58.2±15.2	-2.5±2.8	-24.7±6.2	0	0.011	0.001	0.017	0.011	0.001	0.017	0.011
ΔP(Nd±SD)	0.015	0.017	0.016	0.012	0.016	0.016	0.020	0.014	0.018	0.021	0.015	0.017	0.016	0.012	0.012	0.012	0.012	0.016	0.012	0.016	0.012	0.016	
Eu, µg/L	0.06	0.07	0.08	0.05	0.07	0.07	0.08	0.06	0.07	0.09	0.06	0.07	0.09	0.06	0.07	0.09	0.06	0.07	0.09	0.06	0.07	0.09	
ΔP(Eu±SD)	-0.2±4.4	-6.5±2.9	-3.5±3.5	0	-6.0±3.2	-7.6±1.9	-2.3±2.0	0	-6.7±3.2	-0.2±4.4	-6.5±2.9	-3.5±3.5	0	-6.0±3.2	-7.6±1.9	-2.3±2.0	0	-6.7±3.2	0.004	0.0004	0.009	0.004	0.0004
Gd, µg/L	0.009	0.009	0.011	0.007	0.009	0.009	0.011	0.009	0.009	0.011	0.009	0.009	0.011	0.009	0.009	0.011	0.009	0.011	0.009	0.011	0.009	0.011	
ΔP(Gd±SD)	-1.9±1.5	-0.3±1.6	-4.6±6.5	0	-0.1±3.6	-3.4±3.2	-11.0±4.9	0	-21.5±11.3	-0.1±3.6	-3.4±3.2	-11.0±4.9	0	-0.1±3.6	-3.4±3.2	-11.0±4.9	0	-21.5±11.3	0.011	0.001	0.023	0.011	0.001
Ho, µg/L	0.023	0.025	0.033	0.022	0.026	0.026	0.030	0.022	0.023	0.031	0.023	0.023	0.031	0.023	0.023	0.031	0.023	0.023	0.031	0.023	0.023	0.031	
ΔP(Ho±SD)	0	0	0	-5.2±3.0	-2.1±1.8	0	-2.1±3.5	0	-2.0±5.3	0	0	0	0	-2.0±5.3	0	0	0	-15.6±4.9	-22.9±19.5	0	-15.6±4.9	-22.9±19.5	0
Er, µg/L	0.23	0.24	0.23	0.16	0.23	0.23	0.39	0.28	0.28	0.32	0.23	0.28	0.28	0.32	0.28	0.32	0.23	0.28	0.32	0.23	0.28	0.32	
ΔB(Pb±SD)	0	0	0	-21.3±2.5	-2.0±7.6	-2.4±1.6	-8.2±3.3	-7.2±9.9	-0.8±2.7	0	0	0	0	0	0	0	0	0	0	0	0	0	0
Pb, µg/L	0.046	0.052	0.066	0.058	0.054	0.054	0.064	0.053	0.054	0.061	0.046	0.052	0.066	0.058	0.054	0.054	0.064	0.053	0.054	0.061	0.046	0.052	
ΔP(Th±SD)	0	0	-11.6±2.6	-12.2±22.5	-7.8±3.2	-18.1±5.6	0	-2.0±1.9	0	0	0	0	0	0	0	0	0	0	0	0	0	0	

1177
1178
1179
1180
1181

Table 3. Mean (\pm SD), depth-integrated rates of bio- and photodegradation ($\text{mg C L}^{-1}\text{d}^{-1}$)

Object	$V_{\text{Biodegradation}}$	$V_{\text{Photodegradation}}$
Lake Temnoe		
Forest Lake (Jun)	-0.02 ± 0.0014	-0.19 ± 0.03
Forest Lake (Aug)	-0.031 ± 0.010	-0.067 ± 0.066
Forest Lake (Oct)	-0.042 ± 0.013	0
Ilaskoe Bog continuum (July)		
Piezometer water	-0.17 ± 0.09	-0.33 ± 0.07
Peatland pool	-0.029 ± 0.008	0
Outlet stream (Chernyi)	-0.055 ± 0.043	-0.27 ± 0.043

1182
1183
1184
1185
1186
1187
1188
1189
1190